S/T-rich motif in the DNAJB6 chaperone delays polyglutamine aggregation and the onset of disease in a mouse model

Vaishali Kakkar[1], Cecilia Månsson [2], Eduardo P. de Mattos[1,3], Steven Bergink[1], Marianne van der Zwaag[1], Maria A.W.H. van Waarde[1], Niels J. Kloosterhuis[4], Ronald Melki[5], Remco van Cruchten[2], Salam Al-Karadaghi[2], Paolo Arosio[6], Christopher M. Dobson[6], Tuomas P.J. Knowles[6], Gillian P.Bates[7], Jan van Deursen[8], Sara Linse[2], Bart van de Sluis[4], Cecilia Emanuelsson[2#], and Harm H. Kampinga[1#*]

[1] University of Groningen, University Medical Center Groningen, Department of Cell Biology, Groningen, The Netherlands
[2] Department of Biochemistry and Structural Biology, Center for Molecular Protein Science, Lund University, Lund, Sweden
[3] Department of Genetics, Federal University of Rio Grande do Sul, Porto Alegre, Brazil
[4] University of Groningen, University Medical Center Groningen, Department of Pediatrics, Molecular Genetics, Groningen, The Netherlands
[5] Neuroscience Paris-Saclay Institute, Centre National de la Recherche Scientifique, Gif-Sur-Yvette, France
[6] Department of Chemistry, University of Cambridge, Cambridge, UK
[7] King's College London, Department of Medical and Molecular Genetics, London, UK
[8] Mayo Clinic, Rochester, Minnesota, USA

shared last authors
* To whom correspondence should be addressed at Tel: +31-50-3632903, Fax: +31-50-3632913, email: h.h.kampinga@umcg.nl

Summary

Expansion of CAG repeats in genes leads to debilitating human disorders characterized by protein aggregation due to the corresponding polyglutamine (polyQ) tract in proteins leading to neurodegeneration. The mechanism of aggregation involves primary and secondary nucleation steps and we show how a non-canonical member of the DNAJ-chaperone family, DNAJB6, inhibits the conversion of soluble polyQ peptides into amyloid fibrils by strongly suppressing primary nucleation. This inhibition is mediated by a conserved serine/threonine-rich region in DNAJB6 that provides an array of surface-exposed hydroxyl groups that can bind to polyQ peptides and disrupt the formation of H-bonds that are essential for the stability of amyloid fibrils. We show ~~in addition~~ that the early prevention of polyQ aggregation by DNAJB6 also occurs in living cells and leads to delayed neurite retraction even before aggregates are visible. Importantly, in a mouse model, brain-specific co-expression of DNAJB6 delays polyQ aggregation and relieves symptoms and prolongs life span. DNAJB6 is therefore both a potential target for disease therapy and a tool for unraveling the early events in the onset of polyQ diseases.

Highlights:

- *the chaperone DNAJB6 inhibits polyQ aggregation at sub-stoichiometric ratios*
- *DNAJB6 inhibits primary nucleation and formation of amyloid fibrils*
- *DNAJB6 functionality depends on hydroxyl groups in a unique serine/threonine-rich motif*
- *DNAJB6 reduces aggregation, delays symptoms and prolongs life span in polyQ mice*

eTOC Blurb:

Insights into the mechanism by which DNAJB6, a member of the DNAJ-family of molecular chaperones, inhibits early steps in the formation of polyglutamine amyloid fibrils. A unique serine/threonine (S/T)-rich region in DNAJB6 that exposes an array of hydroxyl groups is crucial for inhibition of amyloid formation. Activity is gradually lost in S/T-to-A substitution variants of DNAJB6 both in vitro and in cells. In a polyglutamine mouse model these inhibitory effects of DNAJB6 result in a delay in disease onset and in increased lifespan.

Introduction

In trinucleotide (CAG) repeat expansion disorders, which include Huntington's disease (HD), spinocerebellar ataxias (SCAs) and spinal and bulbar muscular atrophy (SBMA), proteins containing polyglutamine (polyQ) stretches promote protein aggregation and formation of pathological structures such as amyloid fibrils and their precursors (Chiti and Dobson, 2006; Zoghbi and Orr, 2000). The length of the polyQ expansion is strongly linked with aggregation propensity, and is also inversely correlated with the age at onset of the disease (Gusella and MacDonald, 2000). These findings strongly suggest that aggregate formation triggers disease. Yet the mechanism of aggregation, the surface properties and interactions of the aggregates, and even the mechanistic connection between aggregation and the onset of neurodegeneration are not well understood. Several lines of evidence suggest that it is not the full length polyQ proteins that are aggregation prone, but rather that aggregation is initiated by smaller pieces of the full length proteins, which arise either from alternative splicing (Ramani et al., 2015; Sathasivam et al., 2013) or as a result of protease activation by excitotoxic events (Graham et al., 2006; Koch et al., 2011; Raspe et al., 2009). The proteolytic parts of the protein containing the polyQ expansions can either directly or after further processing via the proteasome into polyQ-peptides (Raspe et al., 2009; Venkatraman et al., 2004), promote the subsequent aggregation of the full-length polyQ proteins and of other Q-stretch containing proteins, including a range of transcription factors (Suhr et al., 2001; Venkatraman et al., 2004; Waelter et al., 2001). Indeed, sequestration within these aggregates of essential transcription factors, or of chaperones and proteasome components (Park et al., 2013; Raspe et al., 2009), appears to be one of the key pathogenic events that contribute to the functional impairment of neurons.

Molecular chaperones generally maintain protein homeostasis in cells (Hipp et al., 2014). Some can bind to unfolded polypeptides and assist their folding and assembly, thereby suppressing non-productive protein-protein interactions and aggregate formation (Balch et al., 2008). Several chaperones are upregulated upon acute stress in a process referred to as the heat shock response (HSR) and that is controlled by the heat shock transcription factor-1 (HSF-1) (Akerfelt et al., 2010). A finding that supports the specific proposition that protein aggregation is a major factor driving polyQ diseases is that activation of HSR delays phenotypic changes in fly and worm models of polyQ diseases (Fujikake et al., 2008; Neef et al., 2010; Warrick et al., 1998). Aggregate formation is, however, not always observed to be reduced under such conditions (Warrick et al., 1998), and in mouse models of polyQ diseases the activation of HSR (Labbadia et al., 2011), or the transgenic expression of individual chaperones such as HSPA1A (Hsp70) (Hansson et al., 2003; Hay et al., 2004) and HSPB1 (Hsp27) (Zourlidou et al., 2007), has generally not been found to delay disease onset or reduce aggregate formation. Moreover, the expression of polyQ proteins per se does not activate the HSR, implying that the protein quality control (PQC) system does not respond to the presence of the protein with the polyQ expansion (Seidel et al., 2012); this finding may explain why the canonical chaperones have been so disappointingly ineffective in polyQ diseases. There are also members of the diverse families of molecular chaperones that are not controlled by the classical HSR (Vos et al., 2008) that may serve in alternative pathways for PQC, and so help to counteract polyQ diseases. Indeed, in a dedicated screen for polyQ modifiers (Hageman et al., 2010) we discovered such members, the two close homologues of the DNAJ chaperone family, DNAJB6 and DNAJB8, both of which are oligomeric in their functional states and non-canonical in their mode of action (Kampinga and Craig, 2010). DNAJB8 (expressed in the testis) and DNAJB6 (expressed in several tissues and especially in the brain) were found to be very efficient suppressors of polyQ aggregation in cell models, irrespective of the protein context in which these expansions reside, either huntingtin exon-1 or

a full length ataxin 3 or the androgen receptor (Hageman et al., 2010). Efficient inhibition of aggregation initiated by polyQ peptides has been observed to occur both in cell free (Månsson et al., 2014a) and in cellular models (Gillis et al., 2013). Yet, the mode of action for the remarkable efficiency of DNAJB6 as a suppressor molecule is not understood, nor whether it translates to protection *in vivo*.

Here, we have addressed the following key questions concerning the mechanism of how DNAJB6 can inhibit polyQ aggregation so efficiently: How does DNAJB6 influence aggregation? What features of DNAJB6 make it so special compared to other chaperones? Is the inhibition of polyQ aggregation by DNAJB6 of any relevance for disease also in a mammalian system? We show that analysis of the kinetics of aggregation reveals the fact that DNAJB6 inhibits early steps in the formation of amyloid fibrils, and that the inhibition activity is mediated by a unique and conserved serine/threonine (S/T)-rich region. In addition, we show that this inhibition activity translates into the prevention of neurite retraction, even prior to formation of inclusions in neuronal cells. Furthermore, in a mouse model of polyQ disease that exhibits the most rapidly progressing features of polyQ pathogenicity we show that DNAJB6 delays the onset of disease, reduces the severity of its consequences and significantly prolongs lifespan.

Results

DNAJB6 inhibits primary nucleation of polyQ peptides.

In order to assess the mechanism by which DNAJB6 inhibits the aggregation of different polyQ containing proteins, we studied formation of amyloid fibrils from a widely used 6.5 kDa polyQ peptide (sequence GAMKSFQ$_{45}$F) by monitoring the kinetic profiles of the thioflavin (ThT) fluorescence changes (Månsson et al., 2014a). Identification of the microscopic mechanism of protein aggregation from the analysis of the corresponding macroscopic kinetic profiles is based on the fact that the formation of amyloid fibrils is the consequence of a series of specific processes, including primary nucleation, fibril elongation, fibril fragmentation and secondary nucleation, all of which are associated with individual reaction rate constants. Moreover, the time evolution of fibril formation can be described by a master equation that includes the contributions of the various individual microscopic processes (Arosio et al., 2014; Cohen et al., 2011a, 2011b). The data obtained by analysis of the kinetics of the aggregation reaction at different concentrations of the polyQ peptide (Fig. 1A) indicate that secondary nucleation plays a key role in polyQ peptide aggregation, and in the generation of the oligomeric species that are likely to be the primary agents of cellular toxicity. Next, the aggregation profiles of the polyQ peptide in the presence of DNAJB6 were analyzed (Fig. 1B, C). The experimental measurements show that DNAJB6 substantially delays the aggregation reaction by increasing the lag-time of aggregation, without a detectable effect on the growth phase of the aggregation reaction (note the parallel curves in Fig 1B, C). The rate constants determined from the kinetic analysis reveal the microscopic events that underlie the macroscopic inhibition of the aggregation process, and shows that DNAJB6 strongly inhibits the primary nucleation step in the aggregation process and that modeling this effect most closely describes its mechanism of action (Fig. 1B). At a molar ratio of polyQ peptide to DNAJB6 monomer of 1:0.1, ~~the data indicate that~~ the rate of primary nucleation is reduced by a factor of 10^9 (Fig. 1F, black bar). However, DNAJB6 also perturbs the secondary nucleation process, even though to a much smaller degree. Whereas this effect alone cannot well describe its full mechanism of action (Fig. 1C), secondary nucleation rates are still reduced by a factor of 50 in the presence of DNAJB6 at 1 1:0.1 ratio (Fig. 1G, black bar). The effects on secondary nucleation pathways are further supported by additional analysis of seeded aggregation reaction (Fig. S1): adding polyQ fibrils to the reaction enhances monomer

aggregation (Fig S1A) and DNAJB6 can also slow down these reactions, the magnitude depending on the percentage of seeds added (Fig. S1B). Including both effects on primary and secondary nucleation steps actually leads to an excellent fit of the experimental data (Fig 1G, black curve underneath green curve: see also next section). To see whether DNAJ6B also delays aggregation at sub-stochiometric ratios in another disease-relevant context, the analysis was also performed with a 14 kDa Htt-Exon 1 construct where the N-terminus contributes to the primary aggregation step, yielding qualitatively similar data (Fig. S2). ~~This analysis shows hat DNAJB6 is most likely to interfere with the nucleation steps in aggregation by sequestering either the monomeric polyQ species or the small oligomeric species that are generated in the key initial stages of the reaction.~~ Given that the inhibitory effects of DNAJB6 are substantial, even at very low sub-stoichiometric ratios, such sequestration cannot simply be a consequence of binding to the monomeric species. We conclude therefore that DNAJB6 interacts with the oligomeric species formed by the primary nucleations.

Loss of inhibition activity in S/T substitution mutational variants of DNAJB6.

Our previous cell biological data revealed the likely importance of a conserved serine-threonine (S/T) rich region in the potent anti-aggregation effects of DNAJB6. Deletion of this region resulted in the loss of anti-aggregation activity, and also to loss of HDAC binding and the oligomeric conformation found in cells (Hageman et al., 2010), and as isolated purified protein (Månsson et al., 2014a). This conserved region in DNAJB6 contains many hydroxyl groups in the side chains of the S/T-residues. Since the low molecular weight compound EGCG, a potent inhibitor of fibril formation, contains exposed hydroxyl groups, which have been proposed to engage in establishing intramolecular hydrogen bonding with polyQ peptides (Ehrnhoefer et al., 2006), and hydroxyl groups in conserved tyrosine residues of the Brichos chaperone are important for inhibiting amyloid formation (Willander et al., 2012). In order to explore the potential importance of the hydroxyl groups in the S/T-rich region of DNAJB6 for its ability to inhibit aggregation we therefore generated a set of mutational variants (Fig. 1D) in which 6, 13 or 18 S/T residues were substituted by alanine residues (referred to as S/T-to-A) and one variant in which the entire S/T-rich region was deleted. Purified DNAJB6 (Fig. S3A) forms oligomers which appear highly dynamic since the subunits exchange on a time-scale of hours (Fig. S3B). In contrast, the DNAJB6 variant M4 in which the entire S/T-region is deleted is structurally perturbed, and the oligomeric conformation is lost (Fig. S3C) as was previously seen in cells (Hageman et al., 2010), implying that M4 cannot be used to determine the functionality of the S/T-region per se. However, all the mutational variants M1-M3, with increasing number of S/T-to-A substitutions, remain oligomeric as judged by native PAGE (Fig. S3C), and are also structurally intact as judged by CD-spectroscopy (Fig. S3D). That M3, the mutational variant of DNAJB6 with largest number of S/T-to-A substitutions, is oligomeric was also confirmed by size exclusion chromatography (Fig. S3E): only a minor shift in the monomer-oligomer equilibrium was found when compared to wildtype DNAJB6. From the ThT fluoresence measurements it was evident that the function, i.e the aggregation inhibition capacity of the wildtype DNAJB6, declined declined as a function of the number of S/T-to-A substitutions and was almost completely lost when all 18 S/T residues are substituted with A residues (Fig. 1E, Fig S5). Detailed analysis of the aggregation kinetics (Fig 1F, G) revealed that the S/T-to-A substitutions affected the ability to inhibit both primary and secondary steps in the aggregation reactions.

Structural modeling of DNAJB6 (Fig. S4) suggested that the array of 18 side-chain hydroxyl groups are exposed on one face of the DNAJB6 monomer (Fig. 1H, highlighted in pink). That these exposed hydroxyl groups indeed affect the binding of DNAJB6 to polyQ is suggested in a

filter trap assay where, after completed ThT fluorescence measurements (Fig. 1E), the content in the wells of the microtiter plate was collected, put onto a filter, washed with 0.1% SDS such that only polyQ fibrils stay on filter and probed for the presence of DNAJB with immunofluorescence (Fig. 1I). Quantitation of the immunofluorescence data indicate that the mutational variants of DNAJB6 without the S/T-rich region were to a smaller extent binding and captured into the polyQ fibrils during their formation, compared to wildtype DNAJB6 (Fig. 1J). Taken together, the data in Fig. 1 demonstrate that the unique S/T-rich region in DNAJB6 is crucial for its ability to bind to polyQ peptides and inhibit their primary nucleation.

DNAJB6 prevents initiation of polyQ aggregation within cells.

In order to explore the stage of the reaction at which DNAJB6 affects aggregation within cells, we compared its effects on the aggregation of intracellular polyQ and assessed how this is accelerated by an extracellular addition to the media of polyQ peptides in aggregated and fibrillar forms. Such species can be taken up by cells and released into the cytosol, by as yet unknown mechanisms, where they can then act as seeds for aggregation of both expanded and non-expanded polyQ proteins in the recipient cells (Ren et al., 2009). An eGFP-tagged exon-1 of the huntingtin protein with a non-pathogenic Q stretch (HttQ23-eGFP) was expressed in cells and formed no aggregates spontaneously within 48 h (Fig. 2B-D), but aggregation was observed to occur during 3-48 h following extracellular addition of polyQ peptides in aggregated and fibrillar form (Fig. 2A, 2C-E), referred to as $[Q45\ seed]_{extra}$ (Fig. 2C-E). DNAJB6 almost completely suppressed aggregation initiated intracellularly by eGFP-tagged exon-1 of the huntingtin protein with a pathogenic Q stretch ($[Htt\text{-}Q74\text{-}eGFP]_{intra}$) without such extracellular addition of seeds (Fig. 2D, lower panel), whereas DNAJB6 was found to only slightly delay aggregation of intracellular HttQ23-eGFP following addition of seeds. This finding, summarized in Fig. 2E as a comparison between the left panel (Htt exon 1-Q74, no seeds) and right panel (Htt exon-1 Q23, extracellular Q45 seeds), indicates that, also in cells, DNAJB6 primarily delays the initial processes in aggregate formation which are circumvented by addition of extracellular polyQ seeds and are in line with our data showing inhibition of key initial stages of the polyQ aggregation by DNAJB6 protein *in vitro* (Fig. 1).

S/T substitutions in DNAJB6 also reduce anti-aggregation potential in living cells.

To test whether the S/T-rich region is crucial for the protective effects of DNAJB6 also within the crowded environment of living cells, we expressed exon-1 of the huntingtin protein with an expanded polyQ stretch (Htt-Q119-eYFP) in HEK293 cells and compared the results with or without co-expression of wildtype DNAJB6 or the S/T-substitution variants. These data showed, in close similarity to the observations in the *in vitro* experiments with purified mutational variants of the DNAJB6 protein (Fig. 1), that the anti-aggregation capacity of DNAJB6 was found to decline with the number of S/T substitutions in DNAJB6 also in cells, by counting the fraction of cells with inclusions (Fig. 3 A, D), and by measuring the formation of high molecular weight aggregates, using SDS-PAGE (Fig. 3 B, E) and through a filter trap assay (Fig. 3 C, F).

DNAJB6 reduces neurite retraction in neuronal cells even before visible aggregate formation.

We next evaluated whether DNAJB6 can suppress polyQ aggregation and reduce the associated toxic effects in neuronal cells. We therefore expressed polyQ in differentiated NG108 cells and compared the results with or without co-expression of DNAJB6. Analysis of polyQ aggregation using the filter trap assay (Fig. 4A, B) or by measuring the formation of high molecular weight aggregates, using SDS-PAGE (Fig. S6A, B) showed that in cells co-expressing DNAJB6, polyQ

aggregate formation was strongly suppressed ~~with a concomitant increase in the level of soluble polyQ (Fig. 3A, B).~~ Immunofluorescence (IF) and live cell imaging revealed that aggregates initially appeared in and around the soma of the cells and then, at later time-points, were also found in the neurites (Fig. 4C, Fig. S6C). Cells with Htt-Q119-eYFP inclusions (IF-detectable aggregates) had fewer processes (Fig. 4D). Cells expressing Htt-Q23-GFP (a non-pathogenic polyQ stretch, in contrast to the pathogenic expanded polyQ stretch in Htt-Q119-eYFP) were unaffected (data not shown), demonstrating that the observed effects were indeed due to the expanded polyQ stretch. In cells with Htt-Q119-eYFP inclusions, there were on average 2.0 processes/cell without DNAJB6; in the few cells showing inclusions when co-expressing DNAJB6 this number was significantly higher (4.1 processes/cell). Importantly, DNAJB6 co-expression increased the number of processes also in cells without detectable aggregates (2.1 processes/cell without DNAJB6; 5.7 processes/cell with DNAJB6)(Fig. 4C, D). In addition, FRAP analysis (Fig. S7) revealed that the mobility of the otherwise diffusely distributed Htt-Q119-eYFP, in areas within the cytosol but outside inclusions, was reduced compared to a GFP control and increased in cells co-expressing DNAJB6. These findings are consistent with the direct action of DNAJB6 prior to the formation of visible inclusions, on species formed at very early stages in the aggregation process. In line with its loss of anti-aggregation activity (Fig. 1, 4), the M3 mutational variant with 18 S/T-to-A substitutions was unable to protect against polyQ-mediated loss of processes (Fig. 4 C, D).

DNAJB6 binds to polyQ via its S/T-rich region in cells and requires its J-domain for interaction with HSP70 and full activity

To confirm early interaction of DNAJB6 with soluble, non-aggregated polyQ species we performed co-immunoprecipitation in NP40 soluble cell lysates. Indeed, significant amounts of polyQ were immunoprecipitated with DNAJB6 (Fig 5A). Near to no co-immunoprecipitation with the M3 mutational variant with 18 S/T-to-A substitutions, which was unable to protect against polyQ-mediated loss of processes, was observed (Fig. 5A) confirming the *in vitro* data (Fig. 1I, J) that the S/T-rich is crucial for substrate binding and hence the anti-aggregation function of DNAJB6.

DNAJ proteins are usually thought to function through interaction with Hsp70, i.e. within the context of the Hsp70 machinery. There is a histidine-proline-aspartate (HPD) motif within the J-domain which is crucial for DNAJ-Hsp70 functional interactions (Kampinga and Craig, 2010). Indeed, DNAJB6 can interact with the Hsp70 family member HSPA1A in cells, as revealed by co-immunoprecipitation analyses (Fig. 5B), whereas a mutant carrying a substitution in the conserved HPD domain (H31Q: converting this motif from HPD to QPD) completely loses its ability to interact with HSPA1A. In contrast, the M3 mutational variant with 18 S/T > A substitutions still fully retained is ability to interact with HSPA1A (Fig. 5B), further supporting the *in vitro* data (Fig S3) that these substitutions had not affected the main structural features of DNAJB6. For wildtype DNAJB6, the H31Q mutation had been shown to only marginally affect the ability of DNAJB6 to delay polyQ aggregation in cells (Hageman et al., 2010). Such independency of Hsp70 is also observed *in vitro* with no enhanced effect by addition of Hsp70 into the reaction mixture with DNAJB6 (Månsson et al., 2014a). However, given the very efficient protection against polyQ aggregation at extremely low stoichiometry, we hypothesized that the capacity of wildtype DNAJB6 to bind to substrates in cells may not have been sufficiently challenged to reveal such Hsp70 dependency. To address this issue further, we introduced an H/Q mutation in the DNAJB6 mutational variant M2 (13 S/T-to-A substitutions, see Fig. 1F) which had considerably reduced, but still some residual anti-aggregation activity compared to wildtype DNAJB6, both *in vitro* (Fig. 1) and when expressed in cells (Fig. 3). This double mutant, with the QPD-mutation in

the already impaired M2 mutational variant of DNAJB6, showed an almost complete loss of inhibitory activity, whereas the QPD-mutation in the wildtype DNAJB6 still inhibited polyQ aggregation to 75% (Fig. 5C-H). This result implies that DNAJB6 is a bona-fide DNAJ protein that ~~in principle~~ has the capability to bind to and collaborate with Hsp70, although such Hsp70 interaction is required only under conditions where the DNAJB6 capacity is limited. Under such conditions Hsp70 might be required to assist in release of the substrate peptides bound to DNAJB6 and thereby recycle DNAJB6. In line, we find that the H/Q mutant of DNAJB6 pulls-down more polyQ than wildtype DNAJB6 (Fig 5A).

In summary, the combined data with purified proteins (Fig.1) and in diverse cellular models (Fig. 2-5) suggest a model in which DNAJB6 strongly suppresses primary nucleation and identifies the S/T-rich region as a functional (sub)domain in the DNAJB6 protein that is responsible for its chaperone activity. The ability of DNAJB6 to inhibit aggregation of polyQ containing proteins relies on direct interaction with the substrate, the polyQ stretch itself, an ability that canonical chaperones – that mainly recognize hydrophobic regions – seem to lack. This explains why DNAJB6 is a much more potent inhibitor of polyQ aggregation than other chaperones, including several other members of the DNAJ protein class, that have so far been investigated (Hageman et al., 2010).

Brain-specific DNAJB6 expression reduces aggregation and delays disease onset in a polyglutamine mouse model.

To study whether or not the highly protective effects of DNAJB6 observed *in vitro* and in cells also translate into neuro-protection *in vivo*, we generated transgenic mice that express the human DNAJB6 under control of the brain-specific nestin promotor (Fig. 6A), with no significant expression in other tissues (Fig. 6B, C). DNAJB6 transgenic mice were born in the expected Mendelian ratios and did not show any overt phenotype. The expression of the human DNAJB6 transgene did not affect the expression of the endogenous mouse DNAJB6 nor of any of the other DNAJs analyzed (Fig. S8). In addition, the HSPA1A (the stress-regulated Hsp70) levels were unaltered in brain and muscle lysates from the transgenic mice (Fig. S9) showing that overexpression of DNAJB6 does not induce a general stress response.

Next, the DNAJB6 transgenic mice were crossed with R6/2 mice expressing exon-1 of the human huntingtin gene, containing 201 ± 1 CAG repeats: this R6/2 model exhibits the most rapidly progressing features of polyglutamine pathogenicity in any mouse model and captures several key aspects of human disease, including early onset motor dysfunction associated with the generation of protein aggregates in the brain, and a substantial reduction in lifespan (Mangiarini et al., 1996; Menalled et al., 2009). ~~Whole brain lysates from R6/2 mice (referred to as HTT) and double transgenic (HTT/JB6) mice were then compared at different ages for the presence of aggregates. The huntingtin aggregates in brain lysates increased over time in the HTT mice (Fig. 6D) in accord with previous studies, but the aggregate load was found to be reduced significantly (by 60% and 30% at week 9 and 12, respectively) in the HTT/JB6 mice co-expressing the DNAJB6 transgene (Fig. 6D,E). Moreover,~~ Immunohistochemical analysis on paraffin-embedded brain sections revealed an age-dependent increase in the formation of nuclear inclusions in the striatum of the HTT mice (Fig. 6D, E) but not in the WT or DNAJB6 transgenic mice (Fig. S10). Importantly, formation of inclusions in the brain was greatly reduced in the double transgenic HTT/JB6 mice at all time-points recorded (Fig. 6D, E). Biochemical detection of aggregates (as high molecular weight smears) in total brain lysates also showed reduction of aggregation in HTT/JB6 mice when compared to HTT mice (Figure S10A), albeit that this effect

was less pronounced since the nestin promoter that was used to drive expression of DNAJB6 is not active in all brain areas.

We next investigated the effect of this reduction in aggregate load in the brain on motor (dysfunction) symptoms. In agreement with earlier data (Mangiarini et al., 1996; Menalled et al., 2009), the HTT mice showed an early decline in rotarod performance, which progressively deteriorated with age. In the HTT/JB6 double transgenic mice, however, this decline was substantially delayed; for example, at 12 weeks of age the latency time to fall for the HTT/JB6 mice (45 s) was double that of the HTT mice (22 s) (Fig. 7A). Also, both hind limb (Fig. 7B) and full body clasping (Fig 7C) observed in the HTT mice were greatly delayed in the double transgenic HTT/JB6 mice; 70% of the HTT mice, but none of the HTT/JB6 mice, showed full body clasping at the age of 12 weeks. Finally, the life span of the HTT/JB6 mice was extended by over 20% when compared to that of the HTT mice (Fig. 7D). This increase in life span is even more remarkable in view of the fact that DNAJB6 expression was exclusively elevated in parts of the brain and not in other tissues (Fig. 6B), as HD aggregates also affect skeletal and cardiac muscle, and aggregation-related progressive muscle atrophy has been reported to be a significant contributor to the impaired motor ability and early death in the R6/2 model (Orth et al., 2003; Ribchester et al., 2004; Sathasivam et al., 1999). We confirmed that aggregates were indeed present in the muscles of R6/2 mice but, consistent with the brain specific DNAJB6 expression, the extent of aggregation in quadriceps skeletal muscle in the HTT/JB6 mice was found to be similar to that in the HTT mice (Fig. S11B). In addition, wasting effects, indicated by muscle weight loss, were found to be similar in both HTT and HTT/JB6 mice (Fig. S11C). Since muscle waste likely contributed to the life span measurements, the potential protective effects of DNAJB6 on lifespan may thus be even greater if DNAJB6 expression was not restricted to the brain.

Discussion

Our present findings have identified a conserved and unique S/T-rich region in DNAJB6, a non-canonical member of the DNAJ-family of molecular chaperones, as a key element in preventing polyQ aggregation and amyloid formation. We show how the capability of DNAJB6 to directly interact with polyQ peptides translates into protection against detrimental effects of polyQ in cells and to the delayed onset of aggregation and neurodegenerative symptoms in polyQ mice, ultimately resulting in a substantial extension of their lifespan.

Conservation of polyQ-aggregation behavior from *in vitro* to *in vivo*.

The kinetics of polyQ-aggregation and the effects on them of DNAJB6 have been measured at a range of concentrations enabling us to utilize the framework of chemical kinetics of the data for understanding the nature and rates of the specific microscopic steps in the mechanism of aggregation (Arosio et al., 2014; Cohen et al., 2015). In particular, the rate of primary nucleation was found to be significantly reduced in the presence of DNAJB6 (Fig. 1), which is expected to delay the formation of aggregates *in vivo* and to reduce the population of the toxic oligomers, particularly at early time points (Arosio et al., 2014; Cohen et al., 2015). The cellular data (Fig. 2-5) and the data acquired from experiments with the transgenic mice (Fig. 6,7) are in agreement with this prediction, providing evidence that, in this polyQ system at least, the aggregation process observed *in vitro* is analogous to that generating the toxicity observed *in vivo*. Inhibition of primary nucleation is the dominant action of DNAJB6, although DNAJB6 was also found to delay secondary nucleation (Fig 1) but to a much smaller extent.

The S/T-rich region in DNAJB6 and role of hydroxyl side chains.

The S/T rich stretch is unique for DNAJB6 and DNAJB8 within the DNAJ family and its deletion has been found to result in a loss of function in aggregation inhibition (Hageman et al., 2010). However, since deletion of the entire S/T-rich region also affected DNAJB6 structure, oligomeric conformation and HDAC binding, it was unclear as to whether or not this stretch was in fact directly involved in suppression of polyQ aggregation. The results described here show that S/T-to-A substitution does not affect the secondary structure and oligomeric conformation of DNAJB6, and demonstrate that the extremely efficient inhibition by DNAJB6 of primary nucleation is totally dependent on this region of DNAJB6, and of the array of 18 hydroxyl side chains that is exposed asymmetrically on one side of the DNAJB6 monomer structure (Fig. 1). This array provides this chaperone with multivalent hydrogen bonding capacity that can be presumed to be the key factor that enables it to directly bind to and suppress amyloid formation by polyQ proteins (Figs. 1, 3-5). Moreover, this is the first identified functional substrate binding domain in a human DNAJ protein.

Comparison of DNAJB6 functionality with that of other heat shock proteins.

Our data also provide an explanation for the findings that DNAJB6 (and DNAJB8) are the most potent suppressors of polyQ aggregation within the human chaperonome (Hageman et al., 2010). The protective effects of DNAJB6 in the aggressive R6/2 polyQ mouse model (Figs. 6, 7) is the largest reported protection so far for any study involving the over-expression of a single human chaperone. Indeed, HSPA1A (Hsp70) and HSPB1 (Hsp27) have been found to be ineffective in this model (Hansson et al., 2003; Hay et al., 2004; Zourlidou et al., 2007), whilst DNAJB2, a DNAJ protein that is related to DNAJB6 but lacks the S/T stretch, leads to modest effects on disease onset (Labbadia et al., 2012). The high potency of DNAJB6 can be attributed to its direct interaction with the amyloid forming polyQ expansions, inhibiting primary and also secondary nucleation (Fig. 1). Other chaperones like HSPA1A (Hsp70) or DNAJB1 (Hsp40) cannot, however, act in this way but may interact with polyQ inclusions after they are formed, for example by binding to exposed hydrophobic groups of the aggregated polyQ proteins. Indeed, Hsp70, DNAJB1 and several small HSPs are often found to decorate the outer rim of polyQ aggregates (Gillis et al., 2013), where they may function to inhibit aggregate growth (elongation), for example to promote the disposal of aggregates by autophagy, as shown for some small HSP chaperones (Carra et al., 2008; Crippa et al., 2010), or to recover sequestered proteins from the polyQ aggregates for refolding or proteasomal degradation, as suggested for the canonical Hsp70 system (Bailey et al., 2002; Howarth et al., 2009). Such chaperone effects would lead to no, or only minor, reductions in the extent of aggregation, but could alleviate some of the down-stream consequences of polyQ protein aggregation and lead to a transient delay of symptoms (Chan et al., 2000; Warrick et al., 1999), although this effect appears insufficient for long-term protection in the above-mentioned mice models.

The finding that, in cells, DNAJB6 and DNAJB8 not only delay aggregation of polyQ containing huntingtin, but also of polyQ containing ataxin-3 and the androgen receptor (Hageman et al., 2010), further supports the conclusion that its action must involve the polyQ stretch itself in a context-independent, generic manner, consistent with its ability to chaperone pure polyQ peptides (this report, Månsson et al., 2014a). For this to happen, it is important to note that the polyQ stretch in the full-length polyQ proteins usually is not exposed and that the full-length polyQ proteins are not intrinsically misfolded, which is another reason why canonical chaperones may not recognize them prior to aggregation, and thus are not very effective in suppressing these diseases. In line with this conclusion, expression of full length polyQ proteins does not trigger the heat shock response (Hageman et al., 2010; Seidel et al., 2012) and the

steady state expression levels of the expanded and non-expanded alleles are identical in cells from polyQ patients (Koch et al., 2011; Zijlstra et al., 2010), strongly indicating that the polyQ expansion does render the protein a target for accelerated degradation as seen, for example, for misfolded disease-associated proteins such as the mutational variants of SOD1 that are responsible for ALS (Crippa et al., 2010), or some of the CFTR mutants that are associated with cystic fibrosis (Villella et al., 2013). For the polyQ expansion to become exposed and initiate aggregation, several lines of evidence have revealed that the full length proteins have to be shortened, either by protease cleavage (Graham et al., 2006) or via alternative splicing (Ramani et al., 2015; Sathasivam et al., 2013), or need to undergo conformational changes such that flanking sequences open up or align the polyQ stretch for β-hairpin-mediated nucleation (Hoop et al., 2014; Kar et al., 2013; Orr et al., 2010; Sivanandam et al., 2011). In addition, or alternatively, polyQ peptides can be generated upon proteasomal degradation that, in a polyQ-length dependent manner, may aggregate and act as seeds for fibril formation (Gillis et al., 2013; Raspe et al., 2009). At this stage DNAJB6, but not canonical chaperones, would be able to prevent such seeds from being formed.

Whereas prevention of polyQ aggregation by DNAJB6 has previously been suggested to be independent of its ability to work within the context of the Hsp70 machinery (Hageman et al., 2010), our current data demonstrate that this idea has to be revised. This activity is not yet fully saturated under the conditions used previously (Hageman et al., 2010), a situation that results from the extremely efficient substrate-binding capacity of DNAJB6 at sub stoichiometric ratios. Our current data with the QPD-M2 double mutant of DNAJB6 (Fig. 5) demonstrate that the additional QPD mutation in the M2 mutational variant of DNAJB6, already compromised in its anti-aggregation activity (Fig. 1), almost completely reduced its ability to prevent polyQ aggregation in cells. This double mutant form of DNAJB6 required Hsp70 for efficient functioning, showing that DNAJB6 indeed is a DNAJ protein with capability to interact with Hsp70. Moreover, these data suggest that DNAJB6 acts to keep polyQ-containing stretches in a form competent for degradation via Hsp70, at the same time releasing DNAJB6 for preventing new primary nucleation reactions. The Hsp70-independent ability of DNAJB6 to delay polyQ aggregation in a cell free system (Månsson et al., 2014a) is not inconsistent with such a model, as the released seeds would not be degraded and thus would not change the substrate-to-chaperone ratio. How the substrates released from DNAJB6 by HSP70 are processed (e.g. by hand-over to either proteases, peptidases or autophagy) is currently under investigation, but the association of DNAJB6 with HDACs (Hageman et al., 2010) suggests that autophagy may play a significant role.

Physiological functions of DNAJB6.

DNAJB6 is expressed ubiquitously, not just in the brain, and DNAJB6 orthologs are found in all metazoans analyzed so far (Hageman et al., 2010). Yet, its precise function under physiological conditions remains to be elucidated. Besides playing a potential role in suppressing unwanted or uncontrolled amyloid formation, some data suggest that DNAJB6 is important during (excessive) protein degradation; for example, DNAJB6 has been suggested to play a role during keratin degradation (Izawa et al., 2000; Watson et al., 2007), which may explain why DNAJB6 knockout mutant mice die due to failures of chorioallantoic fusion (Hunter et al., 1999). In line with this view, expression network analysis (Fig. S12) reveals that DNA expression is strongly associated with catabolic processes. One speculative possibility is that DNAJB6 may play a more general action in preventing amyloid formation by parts of proteins, shorter than full length proteins, that are generated during such catabolic proteolytic events. In line with this idea, it is important to note that mutations in DNAJB6 that cause a dominant heritable form of limb-girdle muscular

dystrophy (Harms et al., 2012; Sarparanta et al., 2012) are associated with congophilic inclusions and vacuolar changes that are specific to amyloid formation in muscle biopsies (Suarez-Cedeno et al., 2014), supporting the proposal that it has an important anti-aggregation role in muscles under physiological conditions.

Specific overexpression of DNAJB6 in the brain has not been found to have deleterious phenotypic effects, at least in the mouse model used here, suggesting that it could be a potentially safe therapeutic target in polyQ diseases. Furthermore, in line with the absence of effects on the general chaperone network in the brain (Figs. S8, 9), the tissue-specific effect of DNAJB6 implies that its upregulation does not lead to cell-non-autonomous effects of the type that have been suggested to occur, for example, with the HSR-regulator DNAJB1 (Popiel et al., 2012). This observation, and the fact that DNAJB6 does not require a simultaneous upregulation of Hsp70 for its chaperone activity, is likely to be a major advantage because altering Hsp70 expression levels has been associated with an increased risk of malignancies (Dai et al., 2007). In addition, DNAJB6 is active in cells with a compromised heat shock response (Hageman et al., 2010), which suggests that it may remain active in aging neuronal cells in which this HSR may be attenuated (Akerfelt et al., 2010)

The ability of DNAJB6 to inhibit the primary nucleation step in the aggregation of polyQ peptides, observed in the present study, appears to be unique amongst the DNAJ chaperones investigated so far. DNAJB6 might, therefore, also play an important role in the context of other human disorders, in addition to those associated with polyQ aggregation, where amyloid formation is an important factor. Such disorders include Alzheimer's disease, the most common cause of age-related dementia, that is initiated by Aβ peptides (Knowles et al., 2014), and type 2 diabetes, in which the cascade initiating aggregation involves IAPP peptides, a major secretory product of β-cells (Westermark et al., 2011). Indeed, we have recently found that DNAJB6 is able to interact with, and delay fibril formation by, the Aβ42 peptide (Månsson et al., 2014b). In conclusion, molecular species that are able to interfere with protein aggregation are of utmost importance for understanding the role of amyloid formation in biology and disease. Further insights into the mechanism by which DNAJB6 inhibits this process will help to understand both the nature of the aggregation process itself and of its inhibition, and may thereby serve as an important lead for future therapeutic developments directed against this family of highly debilitating amyloid diseases.

Experimental Procedures

Recombinant proteins and peptides.

DNAJB6 protein. The residue numbering refers to the amino acid sequence of human DNAJB6 isoform b (UniProt KB accession number O75190-2). DNAJB6 was recombinantly expressed with an N-terminal tag containing six histidines and a tobacco etch virus (TEV) protease cleavage site (tag sequence MHHHHHHGKPIPNPLLGLDSTENLYFQGIDPFT). After TEV-cleavage and removal of the His-tag, the amino acid residues GIDPFT remain at the N-terminal end of the DNAJB6 protein). Substitution mutants were generated with 6, 13 or 18 S/T-to-A substitutions in the conserved S/T-rich region and designated M1, M2, and M3 and one deletion mutant (Δ132-183), with 21 S/T residues and in total 35 residues deleted, and designated M4. Expression of the DNAJB6 protein and its mutational variants was performed at the Lund Protein Production Platform, Lund University, Sweden (http://www.lu.se/lp3). Purification and characterization of the proteins by native electrophoresis and CD spectroscopy was performed as previously described (Månsson et al., 2014a, 2014b). Size exclusion chromatography was performed at a

flow rate of 0.5 ml/min on a Superdex 200 Increase 10/300 GL column (GE Healthcare, Uppsala, Sweden) equilibrated with 20 mM sodium phosphate buffer pH 8 and 150 mM NaCl. ~~The preparation of the polyQ peptide used here for in vitro studies has been described previously (Månsson et al., 2014a) and has the sequence GAMKSFQ$_{45}$F (Q45) attached to the maltose binding protein via a TEV protease cleavage site (referred to as MBP-TEV-Q45), which permits a controlled initiation of the fibril formation reaction following addition of TEV protease.~~

PolyQ peptide. The polyQ peptide was recombinantly expressed as a fusion with maltose binding protein with an N-terminal tag containing six histidines and a tobacco etch virus (TEV) protease cleavage site (MBP-TEV-Q45), in E. coli strain BL21(DE3) (Stratagene, Santa Clara, CA, USA). The protein lysate was loaded onto a 10 ml bed volume Talon metal affinity resin column (Clontech, Saint-Germain-en-Laye, France), equilibrated in 20 mM Tris–HCl, pH 7.5; 100 mM KCl; 20 mM imidazole; 10 % glycerol and 1 mM DTT, and an imidazole gradient (20–500 mM) was applied and the His-tagged MBP-TEV-Q45 was eluted at 200 mM imidazole, and then loaded on the UnoQ6 column (BioRad, Marnes-la-Coquette, France) equilibrated in 20 mM Tris–HCl, pH 7.5; 20 mM KCl; and 1 mM DTT. The column was washed with five bed volumes of the equilibration buffer, and then a KCl gradient (20–500 mM) was applied, and the His-tagged MBP-TEV-Q45 eluted at 200 mM KCl. The protein concentration was determined from its absorbance at 280 nm using an extinction coefficient of 67840 M^{-1} cm^{-1}. This fusion protein was stored at -80°C in aliquots that were thawed just before use, and polyQ peptides were released by addition of TEV protease.

DNAJB6 binding to polyQ evaluated by filter trap assay After assays for DNAJB6 suppression of polyQ aggregation, the amount of DNAJB6, or its mutational variants, bound to the polyQ fibrils were evaluated with a filter trap assay. End products in the wells after the fibrillation assays were mixed 1:1 (volume) with 2 % SDS in PBS (137 mM NaCl, 2.7 mM KCl, 10 mM Na2HPO4 and 1,8 mM KH2PO4) and transferred to a cellulose acetate membrane filter (pore size 0.2 µm, GE Healthcare, Uppsala, Sweden) on a suction device. The membrane filter was washed, to retain only polyQ in fibril form, twice with PBS supplemented with 1 % SDS and once with PBS alone, after which it was blocked by incubation with blocking buffer (LI-COR, Cambridge, UK) for 1h at RT, then incubated with blocking buffer containing 1:1000 polyclonal rabbit anti DNAJB6 (Innovagen, Lund, Sweden) antibodies for 1h at RT after which it was washed with PBS supplemented with 0.1 % Tween-20 (PBS-T) twice for 5 min. Subsequently the membrane filter was incubated with IRDye 800CW goat anti rabbit (LI-COR, Cambridge, UK) in blocking buffer for 1h at RT in the dark before being washed again, dried in the dark and imaged at 800 nm using an Odyssey CLx IR imaging system (LI-COR). IR intensity of the reactions with chaperone was divided by the intensity of control reactions using Image Studio for Odyssey CLx and Classic (LI-COR), which was also used to generate images.

Assay for DNAJB6 suppression of polyQ aggregation. PolyQ fibril formation was analyzed by Thioflavin T (ThT) fluorescence; 15 µM MBP-TEV-Q45 was mixed with DNAJB6 or its mutational variants in two distinct molar ratios (1:0.1 and 1:0.01) of MBP-TEV-Q45 to DNAJB6 and its mutational variants in buffer (55.9 mM NaPB, 143.5 mM NaCl and 1.35 mM KCl, pH 8.0), supplemented with 10 µM ThT for detection of fibril formation and 1.5 ng/ml TEV protease to initiate the reaction. Samples were prepared on ice and 80 µl aliquots were transferred to microplate wells (Corning® 96 well plates, half-area black/clear bottom polystyrene, nonbinding surface, Corning Incorporated Life Sciences, Acton, USA) in triplicate. ThT fluorescence was measured every 120, 150 or 300 s using quiescent conditions at 37°C using a Fluostar Optima

platereader (BMG Labtech, Offenburg, Germany) with excitation at 440 nm and emission at 480 nm. The fluorescence data were normalized, the lowest value in the dataset being set to 0 and the highest to 1 for each reaction separately. The halftimes (t½) and values of the slopes were determined by fitting non-linear sigmoidal dose-response curves to the normalized data. Within each experiment these values were divided by the average values of three replicates of reactions without the chaperone. These ratios were averaged for three independent experiments and the standard error of mean (SEM) was calculated. For analysis of aggregation kinetics, the reaction profiles were fitted by integrated rate laws for nucleation and growth as previously described (Arosio et al., 2014; Cohen et al., 2011a, 2011b), considering rate constants in the absence and presence of different concentrations of DNAJB6 and the mutational variants, where k_n, k_+ and k_2 are the primary nucleation, fibril elongation and secondary nucleation rate constants, respectively.

Kinetic analysis of polyQ aggregation in vitro. To connect the macroscopic measurements with the details of the microscopic mechanism underlying the inhibition of polyQ aggregation by DNAJB6, we applied a recently developed chemical kinetics platform. To this effect, the experimental kinetic data *in vitro* were analysed by using a kinetic model that considers the processes of primary nucleation, elongation and secondary nucleation. The time evolution of the total fibril mass *M(t)* in the presence of both primary and secondary nucleation events is described by the following integrated rate law (Cohen et al., 2011a, 2011b):

$$\frac{M(t)}{M(\infty)} = 1 - \left(\frac{B_+ + C_+}{B_+ + C_+ e^{\kappa t}} \frac{B_- + C_+ e^{\kappa t}}{B_- + C_+} \right)^{\frac{k_\infty^2}{\kappa k_\infty}} e^{-k_\infty t} \quad \{1\},$$

where the kinetic parameters $B_\pm$, $C_\pm$, and κ are functions of the two combinations of the microscopic rate constants k_+k_2 and k_+k_n, where k_n, k_+ and k_2 are the primary nucleation, elongation and secondary nucleation rate constants, respectively. The microscopic aggregation mechanism of the Q45 peptide in the absence of the chaperone was identified by applying Eq. {1} to globally fit the reaction profiles at different concentrations of Q45. The experimental data were taken from (Månsson et al., 2014a) and the reaction orders of primary and secondary nucleation were fixed as 2 based on the scaling of the halftimes with initial peptide concentrations. This global analysis indicated that the aggregation of the polyQ peptides under the conditions explored in the present study is dominated by secondary nucleation, although primary nucleation occurs to generate the initial species that subsequently proliferate by secondary nucleation. The microscopic steps that are inhibited by DNAJB6 were analysed by applying Eq. {1} to describe the macroscopic profiles of the reactions performed in the presence of DNAJB6. The microscopic reaction steps were identified by comparing the set of microscopic rate constants k_+k_2 and k_+k_n required to describe the time evolution of the fibril formation in the absence and presence of DNAJB6.

Structural model of DNAJB6. To generate structural models the DNAJB6 sequence was uploaded to the Robetta server (http://robetta.bakerlab.org, (Song et al., 2013). Intra- and inter-domain crosslinks identified by CXMS were used as distance constraints to filter the structural models and select that with the best fit. Crosslinking experiments were performed in 20 mM sodium phosphate buffer pH 8.0 and 150 mM NaCl. The crosslinking reagents DSSG

(disulfosuccinimidylglutarate, also abbreviated as BS2G for bis[sulfosuccinimidyl]glutarate) and BS3 (bis[sulfosuccinimidyl]suberate), are amine-reactive, water soluble, homobifunctional protein crosslinkers yielding 7.7 Å and 11.4 Å long spacer arms between lysine residues, and were purchased from Creative Molecules Inc. (Victoria, Canada). The DNAJB6 protein concentration was 1 mg/ml. The crosslinking agents were dissolved in distilled water to a concentration of 30 mM immediately before use, and added to a 40 times molar excess of crosslinker to protein. Sample aliquots were incubated with non-isotopically coded or isotopically coded crosslinkers at 37 °C. After 15 min, the crosslinking reaction was quenched by an excess of primary amine by adding 1 M Tris-(hydroxymethyl)-aminomethane to a final concentration of 20 mM. The samples were then subjected to denaturing gel electrophoresis performed using precast 4–12 % NuPAGE® Bis–Tris Gels (Life Technologies Europe BV, Stockholm, Sweden) in MES buffer according to the manufacturer's instructions. Samples were diluted with LDS sample buffer (4×) (Life Technologies Europe BV, Stockholm, Sweden) and solubilized for 10 min at 95 °C. Gels were stained with Coomassie Brilliant Blue G-250 according to the Quick-stain colloidal CBB protocol (Lawrence and Besir, 2009). The band corresponding to crosslinked DNAJB6 monomer was than excised and subjected to in-gel digestion (ratio 1:50 protease to protein) with a combination of trypsin and chymotrypsin (Promega, Madison, WI, USA) at 37 °C. Samples were acidified by adding 2 µl 10 % trifluoroacetic acid (TFA). The resulting peptides were subjected to reversed phase nano-LC prior to mass spectrometric analyses in a LTQ-Orbitrap Velos Pro mass spectrometer (Thermo Fisher Scientific,Hägersten, Sweden) equipped with a nanoEasy spray ion source (Proxeon Biosystems, Odense, Denmark). The chromatographic separation was performed at 40^0C on a 15 cm (75 µm i.d.) EASY-Spray column packed with 3 µm resin (Proxeon Biosystems, Odense, Denmark). The nanoHPLC intelligent flow control gradient was 5–20% solvent B (0.1% (v/v) FA, 100% (v/v) acetonitrile in water) in solvent A (0.1% (v/v) FA in water) for 60 min, and then 20%-40% for 30 min followed with an increase to 90% for 5 min. A flow rate of 300 nl/min was used through the whole gradient. An MS scan (usually 350–2000 m/z) was recorded in the Orbitrap mass analyzer set at a resolution of 60,000 at 400 m/z, 1 × 106 automatic gain control target and 500 ms maximum ion injection time. The MS was followed by data-dependent collision-induced dissociation MS/MS scans on the 8 or 10 most intense multiple charged ions at 15,000 signal threshold, 30,000 automatic gain control target, 300 ms maximum ion injection time, 2.5 m/z isolation width, 10 ms activation time at 35 normalized collision energy and dynamic exclusion, for 30 or 60 s, with a repeat count of 1. The general mass spectrometric conditions were as follows: spray voltage, 2.0 kV; no sheath or auxiliary gas flow; S-lens 60%; ion transfer tube temperature, 275 °C. Raw data were converted to mgf-format by Mascot Distiller (version 2.3) and further filtered to retain only the top 125 most intense peaks per scan with the software MassAI (version August 2014; http://www.massai.dk; ((Peng et al., 2014; Rasmussen et al., 2011). The identification of crosslinks was made with the following search settings: Fragmentation mode: CID, 10 ppm MS accuracy, 0.04 Da MS/MS accuracy, trypsin combined with chymotrypsin as enzyme, 4 allowed missed cleavages, Variable modifications K (BS3-H20 (x-linker)), K (BS3-d12-H20 (x-linker)), K (BS2G-H20 (x-linker)), K (BS2G-d6-H20 (x-linker)), Crosslinkers BS3 (d0/d12) or BS2G (d0/d6), Also xlink modified peptides. The sequences used in data analysis refer to the amino acid sequence for DNAJB6 isoform B (UniProt KB accession number O75190-2).

Cell culture and transient transfections. Human embryonic kidney cells (HEK293) and neuronal cells (NG108, fusion of neuroblastoma and glioma clones) were cultured according to standard protocols in DMEM (Invitrogen, 41966-052) supplemented with 10% fetal bovine serum (Greiner

Bio-One, 758093) and penicillin/streptomycin (Invitrogen, 15140-163). Differentiation in NG108 cells was induced using 1% NECA (Sigma) and 0.1% IBMX (Sigma). Cells were transfected with exon-1 Htt-Q119-eYFP, pcDNA5/FRT/TO DNAJB6-V5 48 h post differentiation, using the Lipofectamine 2000 reagent (Invitrogen, CA, USA) according to the manufacturer's instructions. Transfection rates were ~10% for NG108 cells and > 70% for HEK293 cells; for transfections with multiple constructs, co-expression was always ~ 90%. Immunocytochemistry was performed as described earlier (Hageman et al., 2010). For immune-staining, differentiated cells were additionally stained for βIII-tubulin to visualize neurites.

Cell and tissue extracts and sample preparation for western blotting. HEK293 cells were prepared and treated as described previously (Hageman et al., 2010). ~~For extracellular addition of polyQ peptide in aggregated and fibrillar forms polyQ peptide, the peptides K2Q30K2 and K2Q45K2 were generated as described before (Ren et al., 2009). The peptides were added to the culture medium at a concentration of 1 μM one day after transfection with the plasmids Htt-Q23-GFP or Htt Q47-GFP and DNAJB6-V5. After the indicated time following peptide addition, the cells were washed with PBS and scraped in FTA buffer (10 mM Tris Cl pH8.0, 150 mM NaCl) + 2% SDS and sonicated.~~ Seeding of intracellular expressed Htt-Q23-GFP or Htt-Q74-GFP aggregation in HEK293 cells was induced by addition of extracellular preformed Q_{45} fibrils (1μM) one day after transfection with the plasmids encoding Htt-Q23-GFP or Htt-Q74-GFP with or without plasmids encoding DNAJB6-V5. Preformed Q_{45} fibrils were obtained by incubating soluble Q_{45} (40 μM) in 20 mM HEPES, pH 7.5; 150 mM NaCl and 10% glycerol, at 37°C without shaking. Full assembly into fibrils was achieved within 5h as assessed by SDS-PAGE analysis and electron microscopy. To reduce fibrils length heterogeneity and bundling, preassembled Q_{45} fibrils were sonicated for 20 min on ice in 2-mL Eppendorf tubes in a VialTweeter powered by an ultrasonic processor UIS250v (250 watts, 2.4 kHz; Hielscher Ultrasonic, Teltow, Germany) set at 75% amplitude, 0.5 s pulses. Transmission electron micrographs of fibrillar Q_{45} adsorbed onto carbon-coated 200 mesh grids and negatively stained with 1% uranyl acetate in distilled water for 1 min were acquired using JEOL 1400 transmission electron microscope operated at an excitation voltage of 80kV and equipped with a Gatan Orius CDD Camera (Gatan) (Ren et al., 2009).

Filter trap samples were prepared as described before (Hageman et al., 2010). For mouse tissue extracts and aggregate detection, the tissues were snap frozen in liquid nitrogen immediately after dissection and homogenized (with a pellet pestle for brain tissue and a bead beater for muscle tissue) in RIPA buffer with NaCl (150 mM), igepal cholate (1%), deoxycholate (0.5%), SDS (0.01%) and Tris-HCl (50 mM). A protease inhibitor cocktail, 0.1 M PMSF and 0.5 M DTT were added fresh to the solution. Samples were sonicated and left on ice for 20 min to ensure proper lysis of the cells and release of proteins. Samples were spun at high speed (13 000 rpm) for 15 min and the pellets were discarded. For all the samples, protein content was determined using the DC protein assay (BioRad, Veenendaal, Netherlands) and prepared in SDS-PAGE loading buffer and heated for 5 min at 100°C. Equal amounts of protein (5 μg for NG108 cell extracts and 50 μg for tissue extract) were loaded on 8% (Htt detection) and 12.5% SDS-PAGE gels. The proteins were transferred onto nitrocellulose membranes and probed with the following primary antibodies: anti-GFP (JL-8 Clontech, Leusden, NL); anti-V5 (Invitrogen, CA, USA); anti-DNAJB6 (Abnova, Walnut, CA, USA) and anti-GAPDH (Fitzgerald Industries International, Acton, MA, USA); anti-Htt S829 (generated in the Bates laboratory, London, UK), and subsequently incubated with appropriate HRP-conjugated secondary antibodies (Amersham, Roosendaal, NL) and anti-goat HRP (Santa Cruz Biotechnology, Dallas, Texas, USA).

Confocal microscopy. Confocal images were obtained using a confocal laser scanning microscope (Leica TCS SP8) with a 63X/1.32 oil objective. Images were processed using ImageJ software (http://rsb.info.nih.gov/ij/). As a minor manipulation, a background correction was applied to all parts of the image.

FRAP analysis. Differentiated NG108 cells were transfected with Htt-Q119-eYFP with or without the mRFP-DNAJB6b construct and the V5-DNAJB6 H/Q mutational variant; the plasmid description can be found in (Hageman et al., 2010). 12 h post transfection, cells were observed and images were collected using a Zeiss LSM780 Confocal 65 Laser Scan Microscope 63x/1.3Imm, equipped with incubation chamber with CO_2 and temperature control (all images were recorded at 37^{o}C). An area spanning the cytoplasm was recorded using minimum laser intensity at a frame rate of 1 per s (50 pre-bleach recordings); subsequently the strip was bleached (one iteration at full laser intention) and recorded for 10 s. The values were analysed using Zeiss software in which they were normalized to the pre-bleach pulse; only the post bleach curves are displayed in Figure 3E.

Immunoprecipitation protocols. For the polyQ-DNAJB6 immunoprecipitation, HEK293T cells were co-transfected with pcDNA5/FRT/TO V5-DNAJB6b WT and an empty pcDNA5/FRT/TO mRFP vector (0.9µg each), or 0.1 µg of Htt-Q119-YFP and 0.9 µg of either pcDNA5/FRT/TO V5-DNAJB6b WT, H31Q or M3 constructs. For the Hsp70-DNAJB6 interaction conditions were identical, with the exception that the Htt-Q119-YFP vector was substituted by 0.5 µg of GFP-HSPA1A in the co-transfections with the DNAJB6 constructs. 24 hours after transfection, cells were washed twice with PBS, scraped in 1ml of PBS, and centrifuged for 5 minutes, 1.000 rpm at 4oC. Pellets were resuspended in 500 µl PBS with the cross linker 3,3'-dithiodipropionic acid di(N-hydroxysuccinimide ester) (1 mM final concentration, Sigma-Aldrich) and incubated on ice for 30 min. The crosslinking reaction was stopped by addition of 10 µl of glycine (100 mM) and incubation on ice for 15 min. After centrifugation for 5 min, 1.000 rpm at 4oC, cells were washed with 1 ml PBS, pelleted again and flash-frozen in liquid nitrogen. Five hundred µl of lysis buffer (150 mM NaCl, 50 mM Tris-HCl pH 8.0, 1.5 mM MgCl2, 0.5% NP-40 (v/w), 3% glycerol (v/w), 0.9 mM DTT and complete EDTA-free protease inhibitor cocktail) were used to homogenize the pellets, which were passed 7 times through a 26G needle. Cells were spun for 15 min, 14.000 rpm at 4oC, the supernatant fractions were transferred to new tubes and 30 µl were collected for input measurement before addition of 25 µl of GFP-Trap® magnetic beads (Chromotek, Planegg, Germany). Extracts were incubated at 4oC for 2 h under gentle agitation, followed by one wash with 500 µl of lysis buffer without DTT, one wash with 500 µl of lysis buffer with 300 mM NaCl and four washes with lysis buffer (with DTT and 150 mM NaCl) on a magnetic rack. Beads were resuspended in 25 µl of 2X Laemli buffer with 10% 2-mercaptoethanol and boiled for 5 min. Antibodies anti-GFP (JL-8 Clontech, Leusden, NL), 1:5000 and anti-V5 (Invitrogen, CA, USA), 1:2000, were used for detection on western blots.

Production of DNAJB6 transgenic mice. DNAJB6 transgenic mice were generated as described by van Ree et al (van Ree et al., 2011). PCR-amplified DNAJB6 (human DNAJB6 isoform b, UniProt KB accession number O75190-2) cDNA with a N-terminal Flag tag was cloned into a unique BglII and XhoI site of the Z/EG expression vector, and verified by sequence analysis. A ScaI-linearized vector was transfected into ES cells by electroporation and G418-resistant colonies with high expression levels of Flag-DNAJB6 were selected as previously described (van Ree et al., 2011). ES

cells were karyotyped and injected into C57BL/6 blastocysts to generate chimeric animals. Chimeric males were used for breeding and offspring were screened for the presence of the transgene by PCR. Mice were backcrossed to C57BL/6 for at least 6 generations. To excise the β-geo-stop cassette in neurons, DNAJB6 transgenic mice were bred to Nesting-Cre mice (B6.Cg-Tg(Nes-cre)1Kln/J; Jackson Laboratories, #003771). The R6/2 HD mice (B6CBA-Tg(HDexon1)62Gpb/3J; Jackson Laboratories, #006494) were from the colonies of Gillian Bates.

Mice handling and maintenance. All procedures were performed with approval of the University of Groningen Ethical Committee for Animal Experiments, which adheres to the principles and guidelines established by the European Convention for the Protection of Laboratory Animals. Experiments were carried out on R6/2 mice and *DNAJB6* transgenic mice that were housed in cages 2-3 mice/cage) under conditions of standard cage enrichment and with *ad libitum* access to food and water. Hemizygous R6/2 mice were bred by backcrossing R6/2 HD males to (CBA x C57Bl/6) F1 females (B6CBAF1/OlaHsd, Harlan Olac). The genotyping and CAG repeat measurements were carried out as described previously (Mangiarini et al., 1996) with primers R6/2 fwd/rev & HDAC4 fwd/rev used for genotyping R6/2 mice and 40256 fwd–40261 rev for CAG repeat sizing (Supplementary Table I). The presence of the *DNAJB6* transgene was confirmed by using primer pairs amplifying the human *DNAJB6* transgene, NEO and CRE. The sequences of all the primers used in this study are listed in Supplementary Table I.

Quantitative PCR. Total RNA was extracted from tissue samples by the Trizol method. 1 µg of total RNA was transcribed using M-MLV reverse transcriptase (Invitrogen, Thermo Fisher Scientific Inc., Waltham, MA, USA). The cDNA synthesis was performed with oligo (dT) 12-18 (Invitrogen, Thermo Fisher Scientific Inc., Waltham, MA, USA). Relative changes in transcript levels were determined on the Icycler (Bio-Rad, Hercules, CA, USA) using SYBR green supermix (Bio-Rad, Hercules, CA, USA). Calculations were done using the comparative CT method according to User Bulletin 2 (Applied Biosystems, Foster City, CA, USA). For each set of primers, the PCR efficiency was determined standard curves with different concentration of primers. Primer sequences used in this study are listed in Supplementary Table I.

Immunohistochemistry. Dissected mouse brains and muscles were fixed in 4% buffered formaldehyde, followed by dehydration and then embedded in paraffin and sliced into 5 µm sections. The sections were de-waxed and labelled with the following antibodies: EM48 for Htt aggregates (MAB5374: Millipore, Billerica, MA, USA), secondary biotin carrying antibodies (Dako, Carpinteria, CA, USA), an avidin–biotin–horse radish peroxidase complex (ELITE ABC Kit, Vector Laboratories, Burlingame, CA, USA) and the AEC chromogen was added for visualization under bright field microscopy. Nuclear counterstaining was performed with haematoxylin. Control sections without primary antibodies did not show positive immunostaining.

Behavioural analysis. Behavioural analysis was performed on an accelerating RotaRod (n ≥ 10 for HTT group; n ≥ 9 for HTT/JB6, WT & JB6 group) using female mice as explained previously (Hockly et al., 2003) with small adaptations: i.e. a top speed of 40 rpm over a period of 300 s. To maintain a gap of 4 weeks between the recordings (in order to avoid learning), two cohorts of animals were used. The recordings from 4, 8, 12, 16 weeks served as one cohort and from 6, 10, 14 weeks as another cohort. At each time point, the mice were tested on three consecutive days, for three trials per day. The data are plotted as an average of all the trials for each day. Statistical analysis was performed using two-way ANOVA. Clasping of limbs was measured as described

previously (Chou et al., 2008) with n = 9 for each animal group. The mice were scored for either hind limb clasping (referred to as stage 1: where one of the hind limbs is clasped for over 50% of the time) or full body clasp (referred to as stage 2: where both the limbs were clasped around the abdomen for more than 50% of the time) over different age groups. Statistical analysis was performed using chi-square test which shows significant difference between the groups (*p<0.05, **p<0.005, ***p<0.001). Lifespan was assessed by Kaplan-Meier analysis.

Author Contributions

V.K., H.H.K, B.vd.S, S.B, C.E, and C.M designed and conceived the experiments. V.K., C.M., and E.M. performed the experiments. M.vd.Z., M.A.W.H.v.W., N.J.K., and R.v.C,. provided technical assistance. J.v.D., R.M., G.P.B., provided reagents and animals. V.K. analysed the cell and mice data; C.M., R.v.C, P.A., T.P.J.K., and S.A-K analyzed the *in vitro* data. V.K., H.H.K., C.E, C.M.D and S.L. discussed the results and wrote the manuscript.

Acknowledgments

The cellular and mouse studies were supported by a grant from Senter Novem (IOP-IGE07004), a Discovery Initiative Grant sponsored by the High Q Foundation (Project # 3.1.2) and a Stimulation Grant from the Nederlandse Hersenstichting (project 15F07(2)-58), all awarded to H.H.K., and a Hersenstichting Grant to S.B. (project no. F2013(1)-52). The *in vitro* aggregation work was facilitated by recombinant expression of the DNAJB6 protein performed at the Lund Protein Production Platform, Lund University, Sweden (http://www.lu.se/lp3) and was funded by the LU Research School for Pharmaceutical Science, the Magnus Bergwalls Stiftelse and the Crafoord Foundation (CE), the European Research Council, the Swedish Research Council and the Nanometer Structure Consortium (SL). PA acknowledges the support of the European Community for a Marie Curie Fellowship for career development. TPJK and CMD acknowledge financial support from the BBSRC, the Frances and August Newman Foundation, the European Research Council and the Wellcome Trust. Marije Been, Sophie M. Post and Jeanette F. Brunsting are thanked for their help with the cellular experiments using the DNAJB6 mutants, and Martha Ritsema and colleagues at the CDP unit of the UMCG are acknowledged for their help with rotarod recordings and mouse handling. Part of the microscopy work has been performed at the UMCG Imaging and Microscopy Center (UMIC), which is sponsored by NWO-grants 40-00506-98-9021 (TissueFaxs) and 175-010-2009-023 (Zeiss 2p).

References

Akerfelt, M., Morimoto, R.I., and Sistonen, L. (2010). Heat shock factors: integrators of cell stress, development and lifespan. Nat. Rev. Mol. Cell Biol. *11*, 545–555.

Arosio, P., Vendruscolo, M., Dobson, C.M., and Knowles, T.P.J. (2014). Chemical kinetics for drug discovery to combat protein aggregation diseases. Trends Pharmacol. Sci. *35*, 127–135.

Bailey, C.K., Andriola, I.F.M., Kampinga, H.H., and Merry, D.E. (2002). Molecular chaperones enhance the degradation of expanded polyglutamine repeat androgen receptor in a cellular model of spinal and bulbar muscular atrophy. Hum. Mol. Genet. *11*, 515–523.

Balch, W.E., Morimoto, R.I., Dillin, A., and Kelly, J.W. (2008). Adapting proteostasis for disease intervention. Science *319*, 916–919.

Carra, S., Seguin, S.J., and Landry, J. (2008). HspB8 and Bag3: a new chaperone complex targeting misfolded proteins to macroautophagy. Autophagy *4*, 237–239.

Chan, H.Y., Warrick, J.M., Gray-Board, G.L., Paulson, H.L., and Bonini, N.M. (2000). Mechanisms of chaperone suppression of polyglutamine disease: selectivity, synergy and modulation of protein solubility in Drosophila. Human Molecular Genetics *9*, 2811–2820.

Chiti, F., and Dobson, C.M. (2006). Protein misfolding, functional amyloid, and human disease. Annu. Rev. Biochem. *75*, 333–366.

Chou, A.-H., Yeh, T.-H., Ouyang, P., Chen, Y.-L., Chen, S.-Y., and Wang, H.-L. (2008). Polyglutamine-expanded ataxin-3 causes cerebellar dysfunction of SCA3 transgenic mice by inducing transcriptional dysregulation. Neurobiol. Dis. *31*, 89–101.

Cohen, S.I.A., Vendruscolo, M., Welland, M.E., Dobson, C.M., Terentjev, E.M., and Knowles, T.P.J. (2011a). Nucleated polymerization with secondary pathways. I. Time evolution of the principal moments. J Chem Phys *135*, 065105.

Cohen, S.I.A., Vendruscolo, M., Dobson, C.M., and Knowles, T.P.J. (2011b). Nucleated polymerization with secondary pathways. II. Determination of self-consistent solutions to growth processes described by non-linear master equations. J Chem Phys *135*, 065106.

Cohen, S.I.A., Arosio, P., Presto, J., Kurudenkandy, F.R., Biverstål, H., Dolfe, L., Dunning, C., Yang, X., Frohm, B., Vendruscolo, M., et al. (2015). A molecular chaperone breaks the catalytic cycle that generates toxic Aβ oligomers. Nat. Struct. Mol. Biol. *22*, 207–213.

Crippa, V., Sau, D., Rusmini, P., Boncoraglio, A., Onesto, E., Bolzoni, E., Galbiati, M., Fontana, E., Marino, M., Carra, S., et al. (2010). The small heat shock protein B8 (HspB8) promotes autophagic removal of misfolded proteins involved in amyotrophic lateral sclerosis (ALS). Hum. Mol. Genet. *19*, 3440–3456.

Dai, C., Whitesell, L., Rogers, A.B., and Lindquist, S. (2007). Heat shock factor 1 is a powerful multifaceted modifier of carcinogenesis. Cell *130*, 1005–1018.

Ehrnhoefer, D.E., Duennwald, M., Markovic, P., Wacker, J.L., Engemann, S., Roark, M., Legleiter, J., Marsh, J.L., Thompson, L.M., Lindquist, S., et al. (2006). Green tea (-)-epigallocatechin-gallate modulates early events in huntingtin misfolding and reduces toxicity in Huntington's disease models. Hum. Mol. Genet. *15*, 2743–2751.

Ellerby, L.M., Hackam, A.S., Propp, S.S., Ellerby, H.M., Rabizadeh, S., Cashman, N.R., Trifiro, M.A., Pinsky, L., Wellington, C.L., Salvesen, G.S., et al. (1999). Kennedy's disease: caspase cleavage of the androgen receptor is a crucial event in cytotoxicity. J. Neurochem. *72*, 185–195.

Fujikake, N., Nagai, Y., Popiel, H.A., Okamoto, Y., Yamaguchi, M., and Toda, T. (2008). Heat shock transcription factor 1-activating compounds suppress polyglutamine-induced neurodegeneration through induction of multiple molecular chaperones. J. Biol. Chem. *283*, 26188–26197.

Gillis, J., Schipper-Krom, S., Juenemann, K., Gruber, A., Coolen, S., van den Nieuwendijk, R., van Veen, H., Overkleeft, H., Goedhart, J., Kampinga, H.H., et al. (2013). The DNAJB6 and DNAJB8 protein chaperones prevent intracellular aggregation of polyglutamine peptides. J. Biol. Chem. *288*, 17225–17237.

Graham, R.K., Deng, Y., Slow, E.J., Haigh, B., Bissada, N., Lu, G., Pearson, J., Shehadeh, J., Bertram, L., Murphy, Z., et al. (2006). Cleavage at the caspase-6 site is required for neuronal dysfunction and degeneration due to mutant huntingtin. Cell *125*, 1179–1191.

Gusella, J.F., and MacDonald, M.E. (2000). Molecular genetics: unmasking polyglutamine triggers in neurodegenerative disease. Nature Reviews. Neuroscience *1*, 109–115.

Haacke, A., Broadley, S.A., Boteva, R., Tzvetkov, N., Hartl, F.U., and Breuer, P. (2006). Proteolytic cleavage of polyglutamine-expanded ataxin-3 is critical for aggregation and sequestration of non-expanded ataxin-3. Hum. Mol. Genet. *15*, 555–568.

Hageman, J., Rujano, M.A., van Waarde, M.A.W.H., Kakkar, V., Dirks, R.P., Govorukhina, N., Oosterveld-Hut, H.M.J., Lubsen, N.H., and Kampinga, H.H. (2010). A DNAJB chaperone subfamily with HDAC-dependent activities suppresses toxic protein aggregation. Mol. Cell *37*, 355–369.

Hansson, O., Nylandsted, J., Castilho, R.F., Leist, M., Jäättelä, M., and Brundin, P. (2003). Overexpression of heat shock protein 70 in R6/2 Huntington's disease mice has only modest effects on disease progression. Brain Res. *970*, 47–57.

Harms, M.B., Sommerville, R.B., Allred, P., Bell, S., Ma, D., Cooper, P., Lopate, G., Pestronk, A., Weihl, C.C., and Baloh, R.H. (2012). Exome sequencing reveals DNAJB6 mutations in dominantly-inherited myopathy. Ann. Neurol. *71*, 407–416.

Hay, D.G., Sathasivam, K., Tobaben, S., Stahl, B., Marber, M., Mestril, R., Mahal, A., Smith, D.L., Woodman, B., and Bates, G.P. (2004). Progressive decrease in chaperone protein levels in a mouse model of Huntington's disease and induction of stress proteins as a therapeutic approach. Hum. Mol. Genet. *13*, 1389–1405.

Hipp, M.S., Park, S.H., Hartl, F.U. (2014). Proteostasis impairment in protein-misfolding and -aggregation diseases. Trends Cell Biol. 2*4*, 506-14.

Hockly, E., Richon, V.M., Woodman, B., Smith, D.L., Zhou, X., Rosa, E., Sathasivam, K., Ghazi-Noori, S., Mahal, A., Lowden, P.A.S., et al. (2003). Suberoylanilide hydroxamic acid, a histone deacetylase inhibitor, ameliorates motor deficits in a mouse model of Huntington's disease. Proc. Natl. Acad. Sci. U.S.A. *100*, 2041–2046.

Hoop, C.L., Lin, H.-K., Kar, K., Hou, Z., Poirier, M.A., Wetzel, R., and van der Wel, P.C.A. (2014). Polyglutamine amyloid core boundaries and flanking domain dynamics in huntingtin fragment fibrils determined by solid-state nuclear magnetic resonance. Biochemistry *53*, 6653–6666.

Howarth, J.L., Glover, C.P.J., and Uney, J.B. (2009). HSP70 interacting protein prevents the accumulation of inclusions in polyglutamine disease. J. Neurochem. *108*, 945–951.

Hsu, A.-L., Murphy, C.T., and Kenyon, C. (2003). Regulation of aging and age-related disease by DAF-16 and heat-shock factor. Science *300*, 1142–1145.

Hunter, P.J., Swanson, B.J., Haendel, M.A., Lyons, G.E., and Cross, J.C. (1999). Mrj encodes a DnaJ-related co-chaperone that is essential for murine placental development. Development *126*, 1247–1258.

Izawa, I., Nishizawa, M., Ohtakara, K., Ohtsuka, K., Inada, H., and Inagaki, M. (2000). Identification of Mrj, a DnaJ/Hsp40 family protein, as a keratin 8/18 filament regulatory protein. J. Biol. Chem. *275*, 34521–34527.

Kampinga, H.H., and Craig, E.A. (2010). The HSP70 chaperone machinery: J proteins as drivers of functional specificity. Nat. Rev. Mol. Cell Biol. *11*, 579–592.

Kar, K., Hoop, C.L., Drombosky, K.W., Baker, M.A., Kodali, R., Arduini, I., van der Wel, P.C.A., Horne, W.S., and Wetzel, R. (2013). β-hairpin-mediated nucleation of polyglutamine amyloid formation. J. Mol. Biol. *425*, 1183–1197.

Knowles, T.P.J., Vendruscolo, M., and Dobson, C.M. (2014). The amyloid state and its association with protein misfolding diseases. Nat. Rev. Mol. Cell Biol. *15*, 384–396.

Koch, P., Breuer, P., Peitz, M., Jungverdorben, J., Kesavan, J., Poppe, D., Doerr, J., Ladewig, J., Mertens, J., Tüting, T., et al. (2011). Excitation-induced ataxin-3 aggregation in neurons from patients with Machado-Joseph disease. Nature *480*, 543–546.

Labbadia, J., Cunliffe, H., Weiss, A., Katsyuba, E., Sathasivam, K., Seredenina, T., Woodman, B., Moussaoui, S., Frentzel, S., Luthi-Carter, R., et al. (2011). Altered chromatin architecture underlies progressive impairment of the heat shock response in mouse models of Huntington disease. J. Clin. Invest. *121*, 3306–3319.

Labbadia, J., Novoselov, S.S., Bett, J.S., Weiss, A., Paganetti, P., Bates, G.P., and Cheetham, M.E. (2012). Suppression of protein aggregation by chaperone modification of high molecular weight complexes. Brain *135*, 1180–1196.

Lawrence, A.-M., and Besir, H.U.S. (2009). Staining of proteins in gels with Coomassie G-250 without organic solvent and acetic acid. J Vis Exp.

Mangiarini, L., Sathasivam, K., Seller, M., Cozens, B., Harper, A., Hetherington, C., Lawton, M., Trottier, Y., Lehrach, H., Davies, S.W., et al. (1996). Exon 1 of the HD gene with an expanded CAG repeat is sufficient to cause a progressive neurological phenotype in transgenic mice. Cell *87*, 493–506.

Månsson, C., Kakkar, V., Monsellier, E., Sourigues, Y., Härmark, J., Kampinga, H.H., Melki, R., and Emanuelsson, C. (2014a). DNAJB6 is a peptide-binding chaperone which can suppress amyloid fibrillation of polyglutamine peptides at substoichiometric molar ratios. Cell Stress Chaperones *19*, 227–239.

Månsson, C., Arosio, P., Hussein, R., Kampinga, H.H., Hashem, R.M., Boelens, W.C., Dobson, C.M., Knowles, T.P.J., Linse, S., and Emanuelsson, C. (2014b). Interaction of the molecular chaperone DNAJB6 with growing amyloid-beta 42 (Aβ42) aggregates leads to sub-stoichiometric inhibition of amyloid formation. J. Biol. Chem. *289*, 31066–31076.

Menalled, L., El-Khodor, B.F., Patry, M., Suárez-Fariñas, M., Orenstein, S.J., Zahasky, B., Leahy, C., Wheeler, V., Yang, X.W., MacDonald, M., et al. (2009). Systematic behavioral evaluation of Huntington's disease transgenic and knock-in mouse models. Neurobiol. Dis. *35*, 319–336.

Neef, D.W., Turski, M.L., and Thiele, D.J. (2010). Modulation of heat shock transcription factor 1 as a therapeutic target for small molecule intervention in neurodegenerative disease. PLoS Biol. *8*, e1000291.

Orr, C.R., Montie, H.L., Liu, Y., Bolzoni, E., Jenkins, S.C., Wilson, E.M., Joseph, J.D., McDonnell, D.P., and Merry, D.E. (2010). An interdomain interaction of the androgen receptor is required for its aggregation and toxicity in spinal and bulbar muscular atrophy. J. Biol. Chem. *285*, 35567–35577.

Orth, M., Cooper, J.M., Bates, G.P., and Schapira, A.H.V. (2003). Inclusion formation in Huntington's disease R6/2 mouse muscle cultures. J. Neurochem. *87*, 1–6.

Park, S.-H., Kukushkin, Y., Gupta, R., Chen, T., Konagai, A., Hipp, M.S., Hayer-Hartl, M., and Hartl, F.U. (2013). PolyQ proteins interfere with nuclear degradation of cytosolic proteins by sequestering the Sis1p chaperone. Cell *154*, 134–145.

Peng, L., Rasmussen, M.I., Chailyan, A., Houen, G., and Højrup, P. (2014). Probing the structure of human protein disulfide isomerase by chemical cross-linking combined with mass spectrometry. J Proteomics *108*, 1–16.

Piro, R.M., Ala, U., Molineris, I., Grassi, E., Bracco, C., Perego, G.P., Provero, P., and Di Cunto, F. (2011). An atlas of tissue-specific conserved coexpression for functional annotation and disease gene prediction. Eur J Hum Genet. 19, 1173-1180.

Popiel, H.A., Takeuchi, T., Fujita, H., Yamamoto, K., Ito, C., Yamane, H., Muramatsu, S., Toda, T., Wada, K., and Nagai, Y. (2012). Hsp40 gene therapy exerts therapeutic effects on polyglutamine disease mice via a non-cell autonomous mechanism. PLoS ONE *7*, e51069.

Ramani, B., Harris, G.M., Huang, R., Seki, T., Murphy, G.G., Costa, M. do C., Fischer, S., Saunders, T.L., Xia, G., McEachin, R.C., et al. (2015). A knockin mouse model of spinocerebellar ataxia type 3 exhibits prominent aggregate pathology and aberrant splicing of the disease gene transcript. Hum. Mol. Genet. *24*, 1211–1224.

Rasmussen, M.I., Refsgaard, J.C., Peng, L., Houen, G., and Højrup, P. (2011). CrossWork: software-assisted identification of cross-linked peptides. J Proteomics *74*, 1871–1883.

Raspe, M., Gillis, J., Krol, H., Krom, S., Bosch, K., van Veen, H., and Reits, E. (2009). Mimicking proteasomal release of polyglutamine peptides initiates aggregation and toxicity. J. Cell. Sci. *122*, 3262–3271.

Van Ree, J., Zhou, W., Li, M., and van Deursen, J.M. (2011). Transgenesis in mouse embryonic stem cells. Methods Mol. Biol. *693*, 143–162.

Ren, P.-H., Lauckner, J.E., Kachirskaia, I., Heuser, J.E., Melki, R., and Kopito, R.R. (2009). Cytoplasmic penetration and persistent infection of mammalian cells by polyglutamine aggregates. Nat. Cell Biol. *11*, 219–225.

Ribchester, R.R., Thomson, D., Wood, N.I., Hinks, T., Gillingwater, T.H., Wishart, T.M., Court, F.A., and Morton, A.J. (2004). Progressive abnormalities in skeletal muscle and neuromuscular junctions of transgenic mice expressing the Huntington's disease mutation. Eur. J. Neurosci. *20*, 3092–3114.

Sarparanta, J., Jonson, P.H., Golzio, C., Sandell, S., Luque, H., Screen, M., McDonald, K., Stajich, J.M., Mahjneh, I., Vihola, A., et al. (2012). Mutations affecting the cytoplasmic functions of the co-chaperone DNAJB6 cause limb-girdle muscular dystrophy. Nat. Genet. *44*, 450–455, S1–2.

Sathasivam, K., Hobbs, C., Turmaine, M., Mangiarini, L., Mahal, A., Bertaux, F., Wanker, E.E., Doherty, P., Davies, S.W., and Bates, G.P. (1999). Formation of polyglutamine inclusions in non-CNS tissue. Hum. Mol. Genet. *8*, 813–822.

Sathasivam, K., Neueder, A., Gipson, T.A., Landles, C., Benjamin, A.C., Bondulich, M.K., Smith, D.L., Faull, R.L.M., Roos, R.A.C., Howland, D., et al. (2013). Aberrant splicing of HTT generates the pathogenic exon 1 protein in Huntington disease. Proc. Natl. Acad. Sci. U.S.A. *110*, 2366–2370.

Seidel, K., Meister, M., Dugbartey, G.J., Zijlstra, M.P., Vinet, J., Brunt, E.R.P., van Leeuwen, F.W., Rüb, U., Kampinga, H.H., and den Dunnen, W.F.A. (2012). Cellular protein quality control and the evolution of aggregates in spinocerebellar ataxia type 3 (SCA3). Neuropathol. Appl. Neurobiol. *38*, 548–558.

Sivanandam, V.N., Jayaraman, M., Hoop, C.L., Kodali, R., Wetzel, R., and van der Wel, P.C.A. (2011). The aggregation-enhancing huntingtin N-terminus is helical in amyloid fibrils. J. Am. Chem. Soc. *133*, 4558–4566.

Song, Y., DiMaio, F., Wang, R.Y.-R., Kim, D., Miles, C., Brunette, T., Thompson, J., and Baker, D. (2013). High-resolution comparative modeling with RosettaCM. Structure *21*, 1735–1742.

Suarez-Cedeno, G., Winder, T., and Milone, M. (2014). DNAJB6 myopathy: a vacuolar myopathy with childhood onset. Muscle Nerve *49*, 607–610.

Suhr, S.T., Senut, M.C., Whitelegge, J.P., Faull, K.F., Cuizon, D.B., and Gage, F.H. (2001). Identities of sequestered proteins in aggregates from cells with induced polyglutamine expression. J. Cell Biol. *153*, 283–294.

Venkatraman, P., Wetzel, R., Tanaka, M., Nukina, N., and Goldberg, A.L. (2004). Eukaryotic proteasomes cannot digest polyglutamine sequences and release them during degradation of polyglutamine-containing proteins. Mol. Cell *14*, 95–104.

Villella, V.R., Esposito, S., Bruscia, E.M., Maiuri, M.C., Raia, V., Kroemer, G., and Maiuri, L. (2013). Targeting the Intracellular Environment in Cystic Fibrosis: Restoring Autophagy as a Novel Strategy to Circumvent the CFTR Defect. Front Pharmacol *4*, 1.

Vos, M.J., Hageman, J., Carra, S., and Kampinga, H.H. (2008). Structural and functional diversities between members of the human HSPB, HSPH, HSPA, and DNAJ chaperone families. Biochemistry *47*, 7001–7011.

Waelter, S., Boeddrich, A., Lurz, R., Scherzinger, E., Lueder, G., Lehrach, H., and Wanker, E.E. (2001). Accumulation of mutant huntingtin fragments in aggresome-like inclusion bodies as a result of insufficient protein degradation. Mol. Biol. Cell *12*, 1393–1407.

Warrick, J.M., Paulson, H.L., Gray-Board, G.L., Bui, Q.T., Fischbeck, K.H., Pittman, R.N., and Bonini, N.M. (1998). Expanded polyglutamine protein forms nuclear inclusions and causes neural degeneration in Drosophila. Cell *93*, 939–949.

Warrick, J.M., Chan, H.Y., Gray-Board, G.L., Chai, Y., Paulson, H.L., and Bonini, N.M. (1999). Suppression of polyglutamine-mediated neurodegeneration in Drosophila by the molecular chaperone HSP70. Nat. Genet. *23*, 425–428.

Watson, E.D., Geary-Joo, C., Hughes, M., and Cross, J.C. (2007). The Mrj co-chaperone mediates keratin turnover and prevents the formation of toxic inclusion bodies in trophoblast cells of the placenta. Development *134*, 1809–1817.

Westermark, P., Andersson, A., and Westermark, G.T. (2011). Islet amyloid polypeptide, islet amyloid, and diabetes mellitus. Physiol. Rev. *91*, 795–826.

Willander, H., Presto, J., Askarieh, G., Biverstål, H., Frohm, B., Knight, S.D., Johansson, J., and Linse, S. (2012). BRICHOS domains efficiently delay fibrillation of amyloid β-peptide. J. Biol. Chem. *287*, 31608–31617.

Zijlstra, M.P., Rujano, M.A., Van Waarde, M.A., Vis, E., Brunt, E.R., and Kampinga, H.H. (2010). Levels of DNAJB family members (HSP40) correlate with disease onset in patients with spinocerebellar ataxia type 3. Eur. J. Neurosci. *32*, 760–770.

Zoghbi, H.Y., and Orr, H.T. (2000). Glutamine repeats and neurodegeneration. Annu. Rev. Neurosci. *23*, 217–247.

Zourlidou, A., Gidalevitz, T., Kristiansen, M., Landles, C., Woodman, B., Wells, D.J., Latchman, D.S., de Belleroche, J., Tabrizi, S.J., Morimoto, R.I., et al. (2007). Hsp27 overexpression in the R6/2 mouse model of Huntington's disease: chronic neurodegeneration does not induce Hsp27 activation. Human Molecular Genetics *16*, 1078–1090.

\

Legends to the Figures

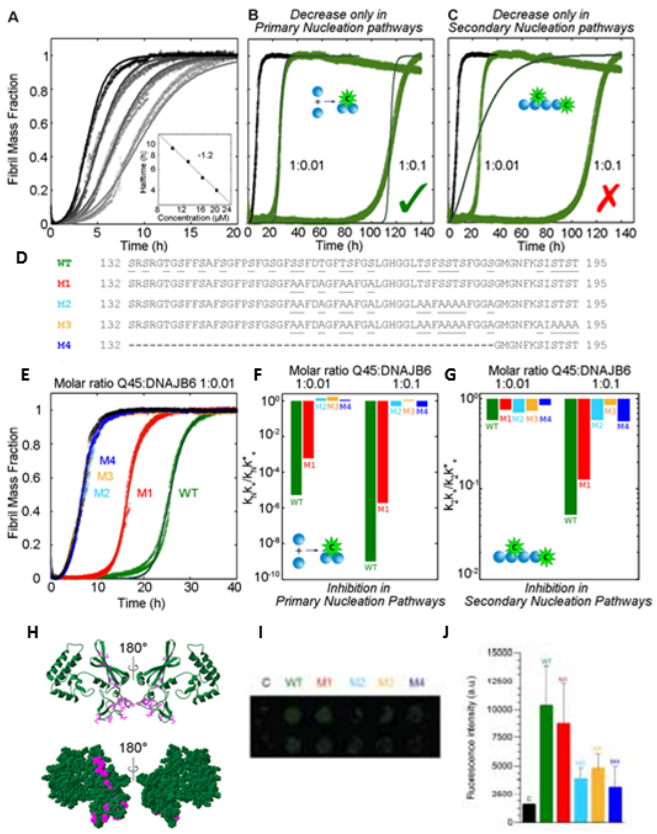

Figure 1: Aggregation suppression mechanism of DNAJB6 and its mutational variants showing that the S/T-rich region is a key structural feature for interactions with polyQ nuclei and inhibition of primary nucleation events. (**A**) Kinetic profiles of the concentration-dependent aggregation of the polyQ peptide at concentrations of 10, 12.8, 16 and 20 µM monitored by ThT fluorescence. Continuous lines represent global fitting of the integrated rate laws to the data according to the equations described in the Methods section. The inset shows the scaling of the half-time with peptide concentration, the value of which indicates the dominance of a secondary nucleation mechanism (34-36). **(B)** Kinetic profiles of the aggregation of 15 µM polyQ peptide in the absence (black) and presence of DNAJB6 (green) at molar ratios of polyQ:DNAJB6 of 1:0.01 or 1:0.1; the thin line represents the fit of the kinetic profiles according to Eq. {1} where only primary nucleation pathways are specifically inhibited (compare to (C)). **(C)** Kinetic profiles as in (B), showing that the delay in the aggregation kinetics observed in the presence of DNAJB6 cannot be described by the integrated rate laws when secondary nucleation pathways alone are specifically suppressed (thin line), confirming that the inhibition activity of DNAJB6 results from its ability to interfere with primary nucleation events ~~(compare to (B)).~~ **(D)** Amino acid sequences of wild-type (WT) DNAJB6 with the S and T residues underlined, and of the mutational variants (M1-M3) with 5, 13 and 18 S/T-to-A substitutions underlined, and of a Δ132-183 deletion mutant variant (M4). (**E**) Kinetic profiles of the aggregation of polyQ peptide (Q45) at a concentration of 15 µM in the presence of DNAJB6 WT (green) or its mutational variants M1 (red), M2 (turquoise), M3 (orange), and M4 (blue) at molar ratios of polyQ to DNAJB6 of 1:0.01 and 1:0.1. The continuous lines represent fits of the integrated rate laws to the data in which inhibition of both primary and secondary nucleation events has been considered simultaneously. **(F, G)** The decreases in the rates of primary nucleation and secondary nucleation, respectively, corresponding to the reaction profiles in (E) for WT DNAJB6 and for the M1-M4 variants, all normalized to the values in the absence of chaperone. The fluorescence data used for all kinetic analyses are presented in Fig. S5. **(H)** Structural model of a DNAJB6 monomer, generated as described in Fig. S4, showing the conserved serine (S) and threonine (T) residues (pink) exposed on one side of the DNAJB6 structure. **(I)** The amount of DNAJB6 and mutational variants M1-M4 of DNAJB6 binding to and captured in polyQ fibrils trapped on filter and probed by immunofluorescence (starting concentrations 15 µM polyQ peptide; upper row 1.5 µM DNAJB6 or variants, lower row 0.15 µM DNAJB6 or variants). (**J**) Quantitation of immunofluorescence data in (I); data from 3 experiments (mean ± SD).

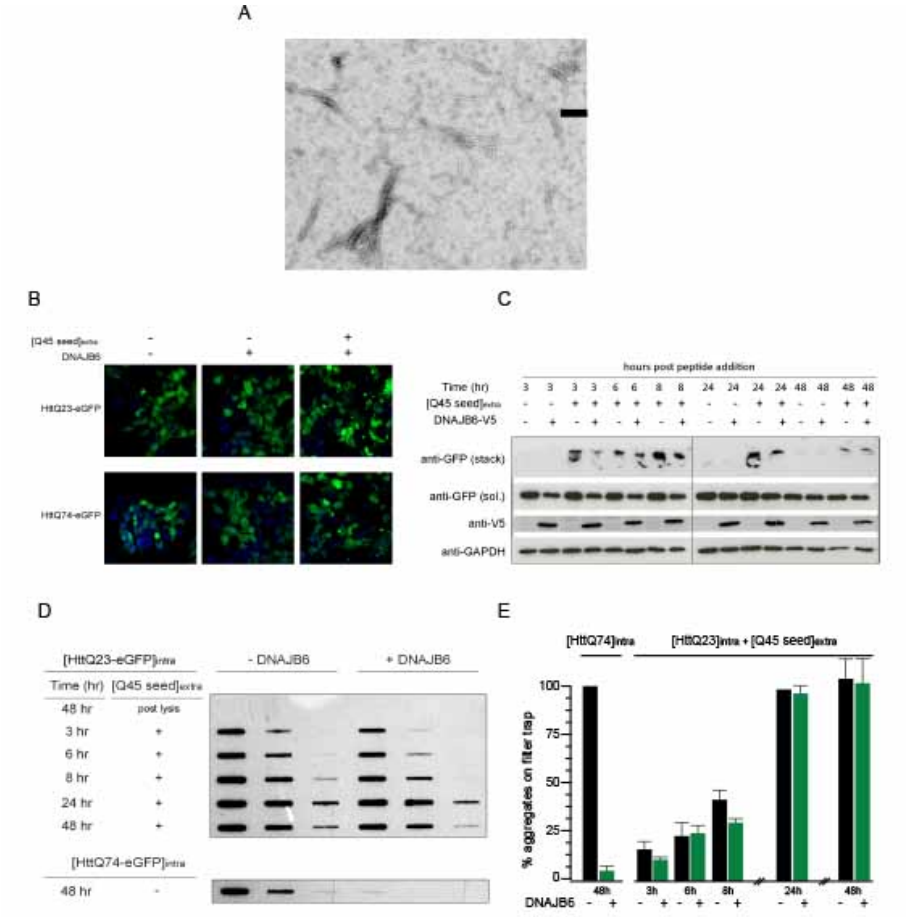

Figure 2: Comparison of the effects of DNAJB6 on seeded and non-seeded aggregation in cells. HEK293 cells expressing Htt-Q23-eGFP or Htt-Q74-eGFP intracellularly, with or without V5-DNAJB6 co-expression, were exposed to 1 µM aliquots of polyQ peptide in aggregated and fibrillar forms ($[Q45\ seeds]_{extra}$) that was added to the medium. **(A)** EM image of the Q45 seeds used. **(B)** Representative confocal pictures of cells co-transfected with DNAJB6 and HttQ23-eGFP (green) or HttQ74-eGFP (green), incubated without (-) or with (+) $[Q45\ seeds]_{extra}$ in the medium. DAPI staining is shown in blue. **(C)** Western blots of the same cell extracts as in panel (B). Nitrocellulose membranes were probed with the antibodies indicated. **(D)** Filter trap assay of the same cell extracts as in panel (A), taken at the indicated time points after the addition of the $[Q45\ seeds]_{extra}$. Three serial five-fold dilutions were loaded onto cellulose-acetate membranes and probed with anti-GFP antibodies to detect aggregation of the intracellularly expressed Htt-Q23-eGFP$_{intra}$ or Htt-Q74-eGFP$_{intra}$. As a control, $[Q45\ seeds]_{extra}$ were directly added after lysis (post lysis) and showed no aggregates. Cells expressing Htt-Q74-eGFP$_{intra}$ show the effective suppression of intracellularly generated aggregates by DNAJB6, without the addition of polyQ peptide in aggregated and fibrillar forms ($[Q45\ seeds]_{extra}$). **(E)** Quantification of the data in panel C; data are the mean ± s.e.m. of 3 independent experiments.

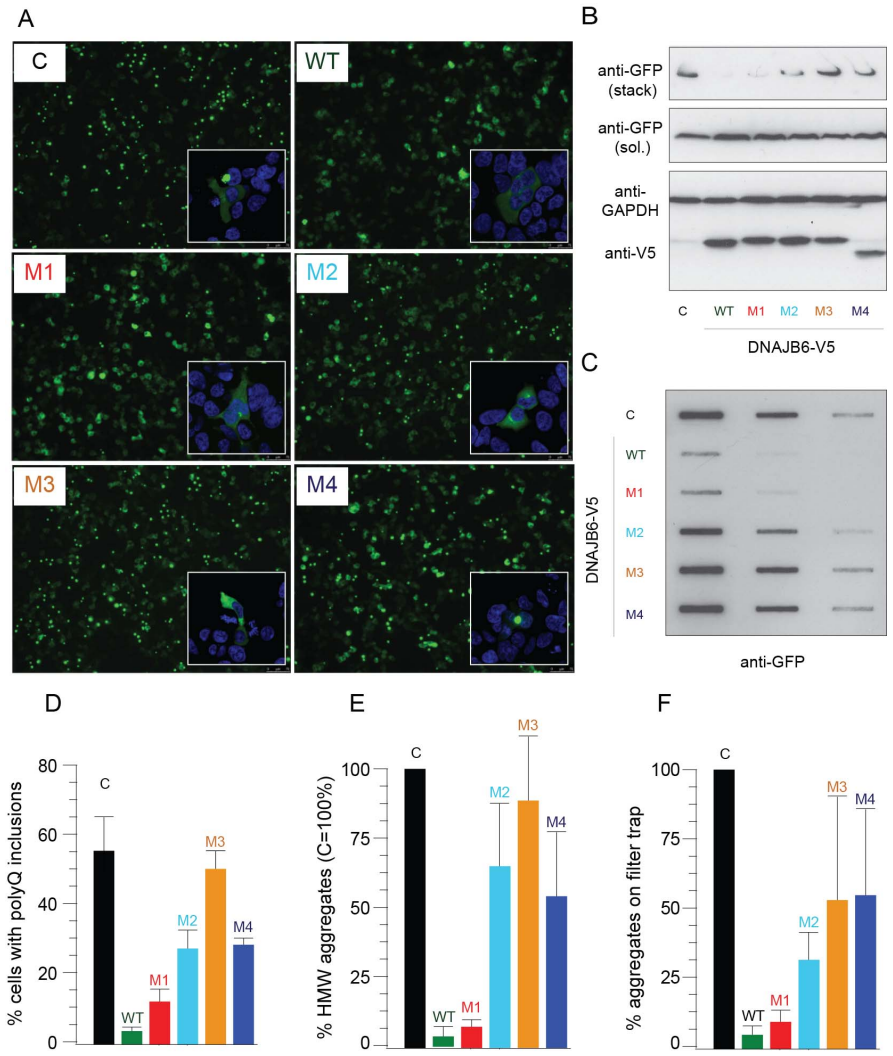

Figure 3: Effects of mutations in the S/T-rich region of DNAJB6 on its ability to prevent aggregation of polyQ in cells. HEK293 cells were transfected with exon-1 Htt-Q119-eYFP (Htt-Q119) without (C, black) or with the wildtype V5-DNAJB6 (WT, green) or the mutational variants having 5 (M1, red), 13 (M2 (turquoise) or 18 (M3, orange) S/T-to-A substitutions in the S/T-rich region of DNAJB6, or a Δ132-183 deletion mutational variant (M4, blue) (see figure 1F). Samples were analyzed 24 h after transfection. **(A)** Representative immunofluorescent pictures of cells transfected with HttQ119-eYFP without (C) or with the wildtype (WT) or the various DNAJB6 mutational variants (M1-M4). **(B)** Western blot of cell extracts. Nitrocellulose membranes were probed with the antibodies indicated, showing expression of the wild type DNAJB6 (WT) and the M1-M4 mutational variants using an anti-V5 antibody. Soluble (sol) and aggregated Htt-Q119-eYFP (stack) (anti-GFP) are also depicted. GAPDH is provided as a loading control. **(C)** Serial five-fold dilutions of the same extracts as in panel B were loaded onto cellulose-acetate membranes and probed with an anti-GFP antibody to detect aggregation Htt-Q119-eYFP. **(D)** Quantitative analysis of the images in panel A, expressing the fraction of cells containing inclusions (2 experiments, each scored by at least 3 independent observers and then averaged). **(E)** The amount of high molecular weight aggregated (HMW) polyQ proteins in panel B relative to cells without chaperones (= 100) from 2 independent experiments (mean ± SD). **(F)** The amount of aggregates captured on cellulose acetate (panel C) relative to cells without chaperones (= 100) from 2 independent experiments (mean ± SD).

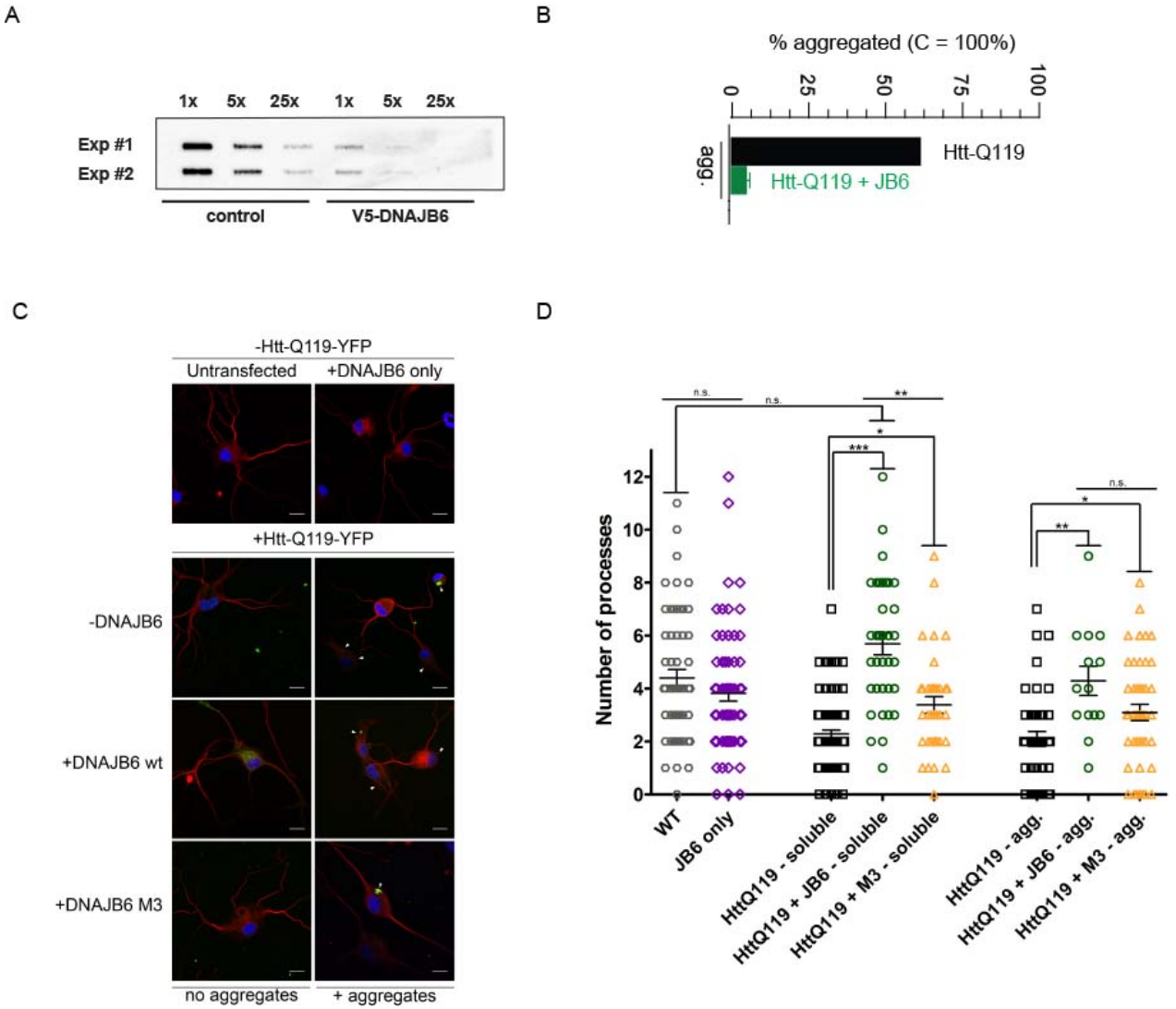

Figure 4: DNAJB6 suppresses the formation of polyQ aggregates and the effect of polyQ expression on neurite formation even before histologically visible aggregation in neuronal cells. Differentiated NG108 cells were transfected with exon-1 Htt-Q119-eYFP (Htt-Q119) with or without V5-DNAJB6 or the V5-tagged DNAJB6 M3 variant with 18 S/T-to-A substitutions. **(A)** Serial five-fold dilutions of the cell extracts in SDS-buffer were loaded onto cellulose-acetate membranes and probed with an anti-GFP antibody to detect aggregation Htt-Q119-eYFP and **(B)** quantified by densitometry (mean + SD of 2 experiments). (**C)** Representative confocal images of differentiated NG108 cells co-transfected with Htt-Q119-eYFP (green) and DNAJB6 with additional staining of β-III tubulin (red) and DAPI (blue). **(D)** Individual cells (approx. 60 cells per condition) were manually counted to identify neurite (dendritic) processes. Cells with and without aggregation of polyQ were scored independently. *P<0.05, **P<0.01, ***P<0.001; Kruskal-Wallis test with Dunn's *post hoc* test. **(E)** FRAP analysis for NG108 cells expressing Htt-Q119-eYFP alone or together with RFP-DNAJB6 or the V5-DNAJB6 H/Q mutant (that is unable to interact with Hsp70), analyzed 12 h post transfection and before the aggregates were visible.

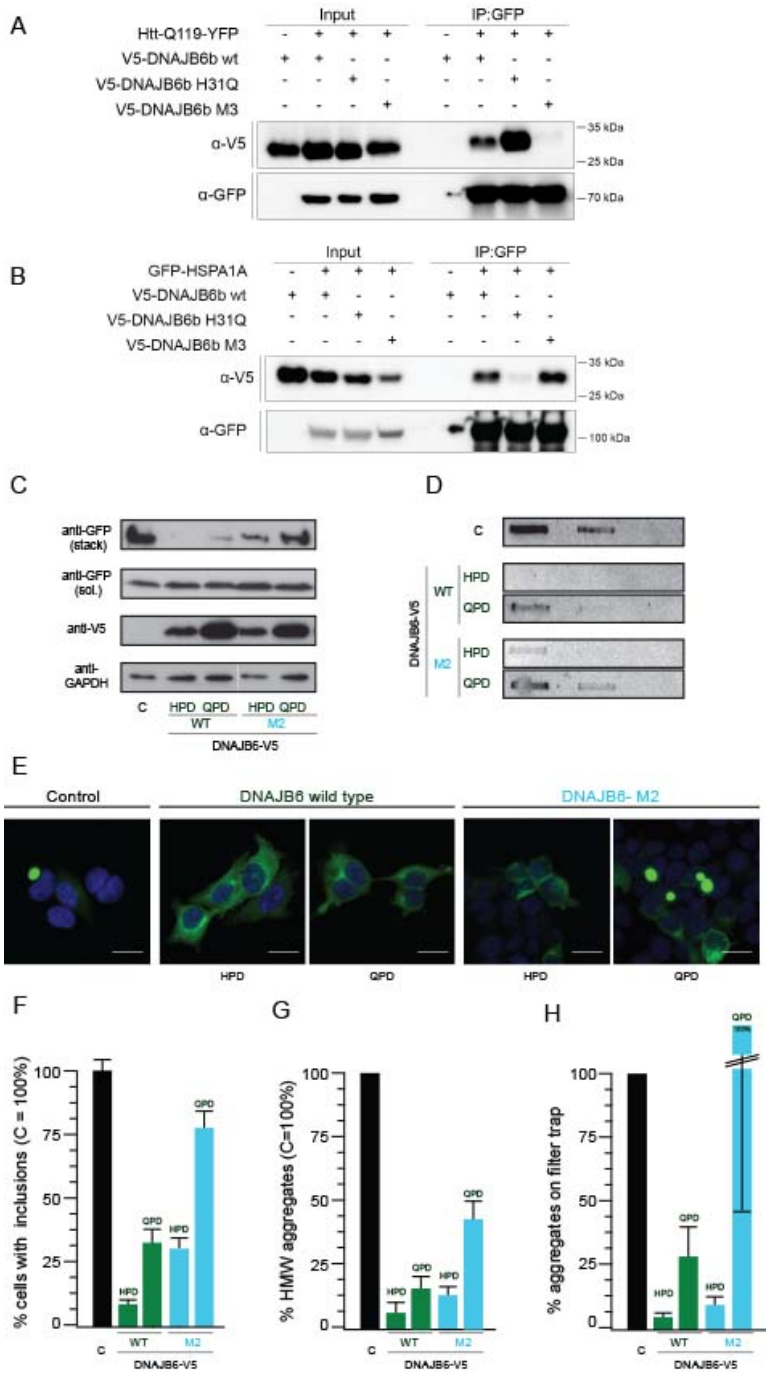

Figure 5: Effects of an HPD mutation on the ability of DNAJB6 to prevent aggregation of polyQ in cells. **(A)** HEK293T cells were co-transfected with Htt-Q119-YFP constructs with either an empty vector or with V5-DNAJB6b WT, V5-DNAJB6b H31Q or V5-DNAJB6b M3 constructs. Cell lysates were treated with a chemical cross-linker and cross-linked material (input) was precipitated using GFP-Trap magnetic beads (IP:GFP) and analysed by westerns blotting. **(B)** Same as A, but using GFP-tagged HSPA1A. **(C-F)** HEK293 cells were transfected with exon-1 Htt-Q119eYFP (Htt-Q119) without (C, black) or with the wildtype V5-DNAJB6 (WT-HPD, green solid), DNAJB6 with a mutation in the HPD motif of the J-domain that disrupts its interaction with Hsp70 (WT-QPD, green open) or with the DNAJB6 mutational variant with 13 S/T-to-A substitutions in the S/T-rich region, either alone (M2-HDP, turquoise solid) or combined with a mutation in the J-domain (M2-QDP, turquoise open). Samples were analyzed 24 h after transfection. **(C)** Western blot of extracts from cells co-transfected with exon-1 Htt-Q119-eYFP (Htt-Q119) and the indicated DNAJB6 variants. Nitrocellulose membranes were probed with the antibodies indicated, showing expression of the different DNAJB6 variants using an anti-V5 antibody, soluble (sol) and aggregated Htt-Q119-eYFP (stack) depicted using an anti-GFP antibody and an anti-GAPDH antibody provided as loading control. **(D)** Serial five-fold dilutions of the same extracts as in panel B were loaded on cellulose-acetate membranes and probed with an anti-GFP antibody to detect aggregated Htt-Q119-eYFP. **(E)** Representative immunofluorescent pictures of cells transfected with HttQ119-eYFP without or with the various DNAJB6 constructs. **(F)** Quantitative analysis of the images like in panel D, expressing the fraction of cells containing inclusions from 4 experiments, each scored by at least 3 independent observers and then averaged (mean ± sem). **(G)** The amount of high molecular weight aggregated (HMW) polyQ proteins in panel B relative to cells without chaperones (=100) from 3-5 independent experiments (mean ± sem). **(H)** The amount of aggregates captured on cellulose acetate (panel C) relative to cells without chaperones (= 100) from 3-5 independent experiments (mean ± sem).

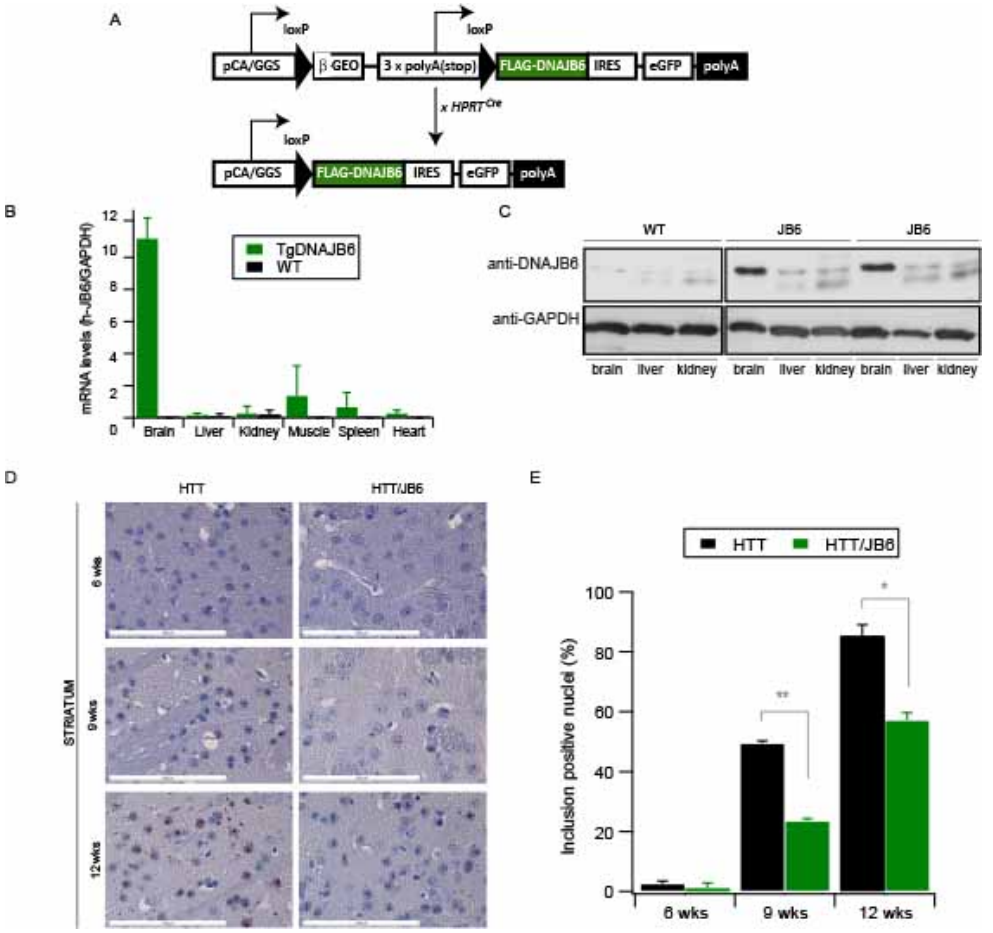

Figure 6: Generation of DNAJB6 transgenic mice and the reduction of HTT aggregate formation in mouse brains. (A) Floxed DNAJB6 transgenic mice were produced as described in the Methods and Results sections and the active transgene was generated after crossing with Nes-CRE mice for specific expression of DNAJB6 in the brains of the animals. **(B)** mRNA levels of the human DNAJB6 transcript relative to GAPDH from a range of tissues from both DNAJB6 transgenic (*TgDNAJB6*: green bar) and wild type (WT: black bar) animals. **(C)** Level of hDNAJB6 protein expression in the brain, liver, and kidney in two TgDNAJB6 mice and one WT mouse. ~~**(D)** Huntingtin aggregation in whole brain lysates was found to be reduced in *HTT/JB6* double transgenic mice compared to *HTT* mice at all time points. The S829 antibody was used to detect both HTT aggregates (agg: in stacking gel) and soluble HTT (sol). **(E)** Relative levels of insoluble HTT were plotted using GAPDH as a loading control and setting values for the HTT mice at 100% (± sem) for each time point (n=3 for each group). The statistical significance was analysed using an independent t-test (*** P=0.0005, ** P=0.007).~~ **(D)** Representative immunohistochemical images of the striatum of *HTT* and *HTT/JB6* mice at various time points. Hematoxylin was used as a nuclear counterstain (blue) and EM48 as a means of visualizing HTT aggregates (brown). Scale bar =: 100 µm. **(E)** The percentage of inclusion positive nuclei; values are the mean ± sem from 3 animals per group; for each sample, 30-40 nuclei were counted for HTT aggregates. The statistical significance of the results was analyzed using an independent t-test (**P<0.008, *P<0.05).

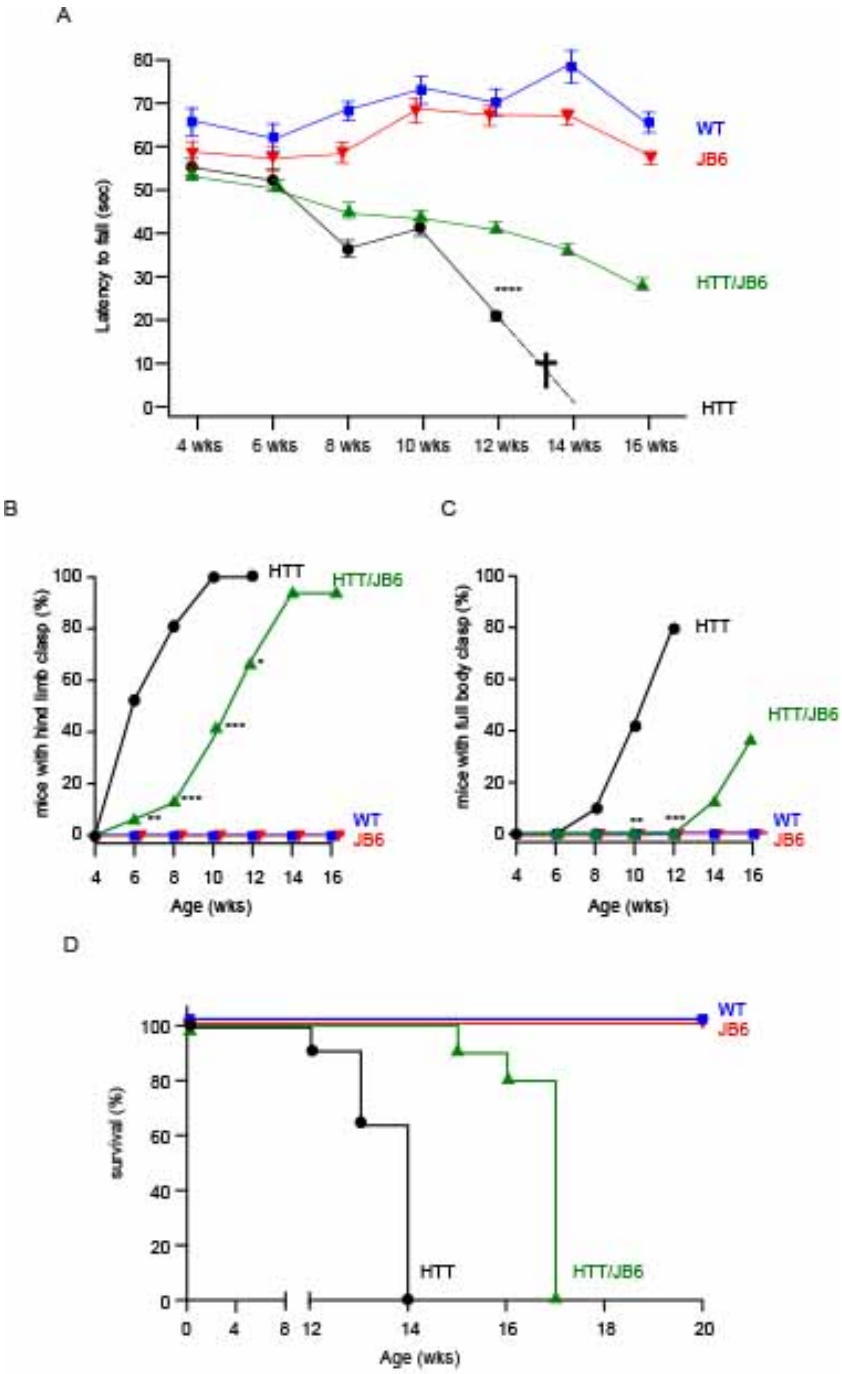

Figure 7: Effect of DNAJB6 overexpression on disease onset in an R6/2 mouse model of HTT disease. Control wildtype mice (WT: bleu), DNAJB6 transgenic mice (JB6: red), R6/2 mice (HTT: black) and R6/2 mice x DNAJB5 mice (HTT/JB6: green) were analyzed at the indicated time points for: **(A)** Performance on a rorarod, where the latency time that each animal stayed on the rotating rod before falling was monitored in 3 trials per day for 3 consecutive days for each group. The mean ± sem values of the three trials on each day are plotted. Data were tested for normality by using Komogorov-Smirnov normality test and was compared using two-way ANOVA followed by a Holm-Sidak Post-hoc test. Data was extremely significant for HTT versus HTT/JB6 at 12 wks of age (****p<0.0001). No statistical differences were found between control groups (WT and JB6). **(B)** Hind limb clasping and **(C)** full body clasping scored between HTT and HTT/JB6 group. Chi-Square test for contingency was performed representing *p<0.05, **p<0.005, ***p<0.001 significance. **(D)** Kaplan-Meier plot for progression free survival (>20% weight loss). Animals with more than 20% weight loss were sacrificed (50% survival is at 13.5 weeks for HTT mice and 17.5 weeks for HTT/JB6 mice, implying a 23% increase in life span for the latter).<Vaishali: please add statement on the statistics here>